From quasars to microquasars

jetted AGN

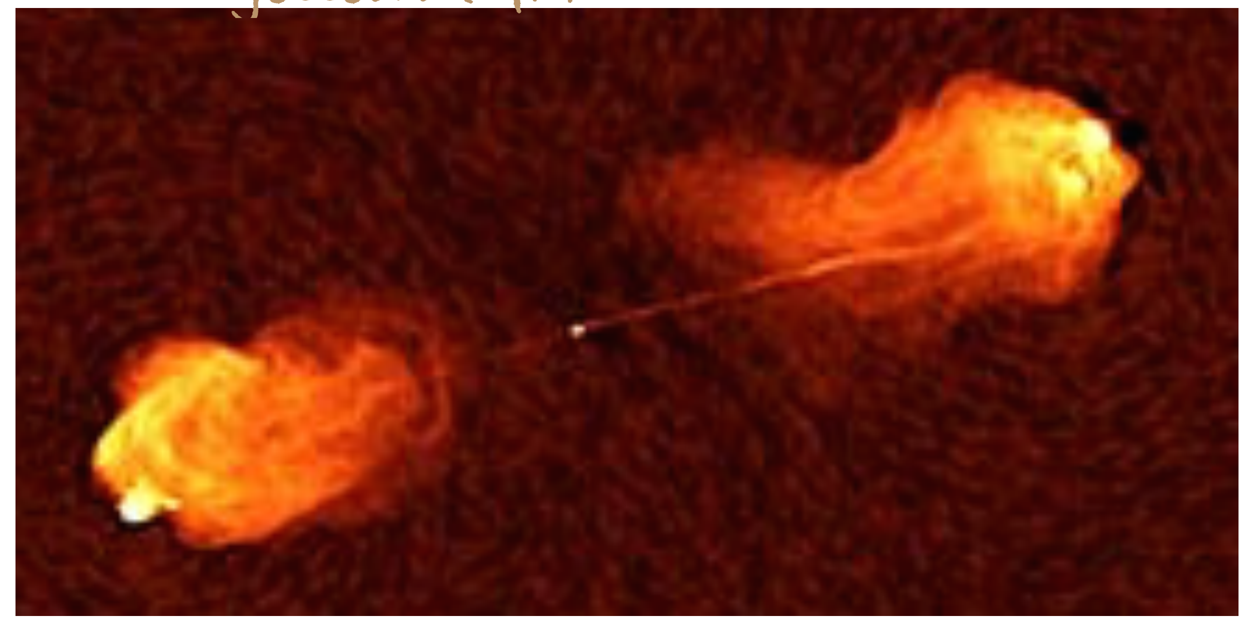

BH masses: 10^8-10^9 M_{sun}
duty cycles: 10^7 yrs

stellar binaries

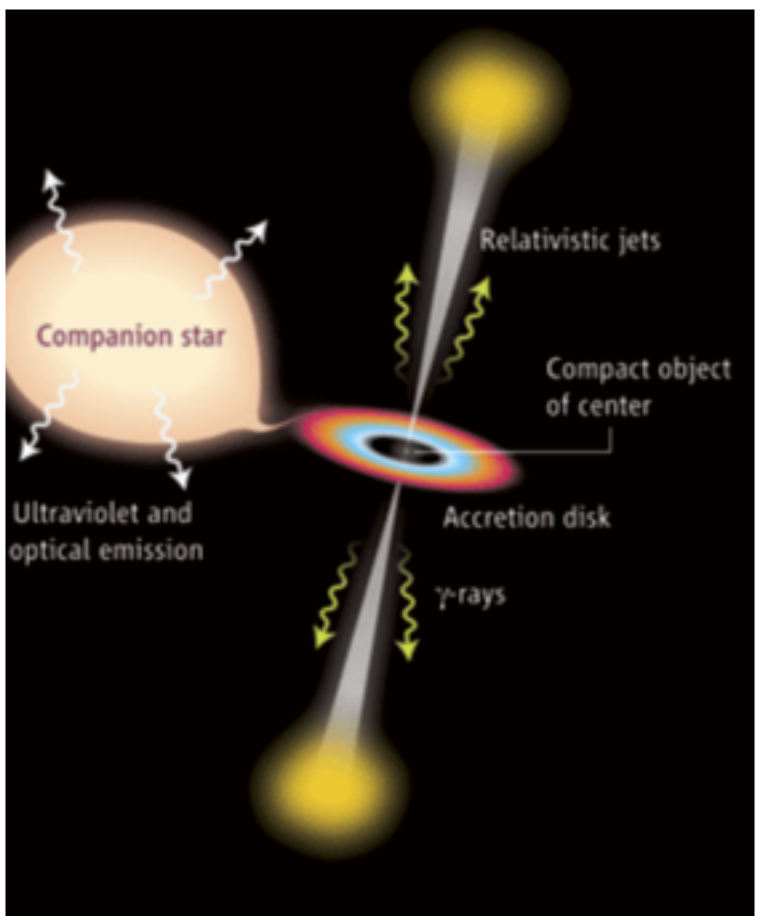

BH masses: 10s M_{sun}
duty cycles: month-to-yrs
L_{radio}~10^{28-32} erg/s

Radio Luminosity

Mass/variability timescales

Jet Flavors in Microquasars

compact, persistent radio jets (~10 AU)

transient, relativistic radio jets (~100s AU)

large scale jets, hot spots (up to ~10s pc)

& radio lobes/ cavities

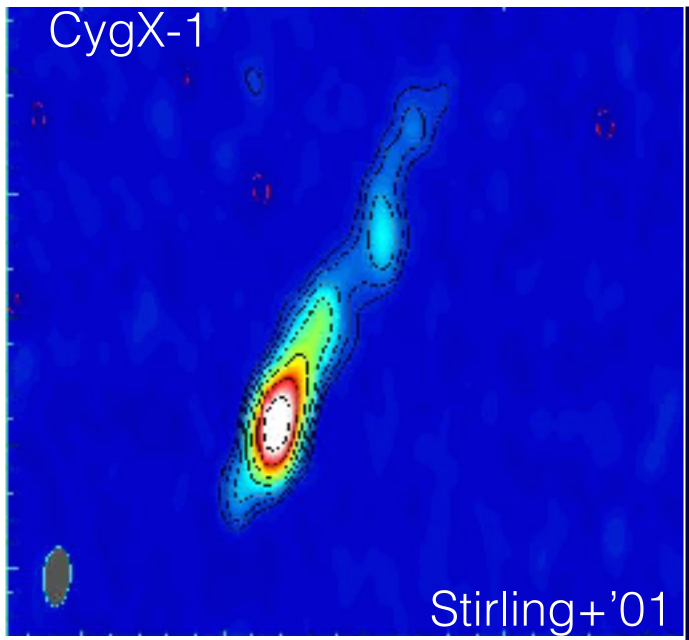

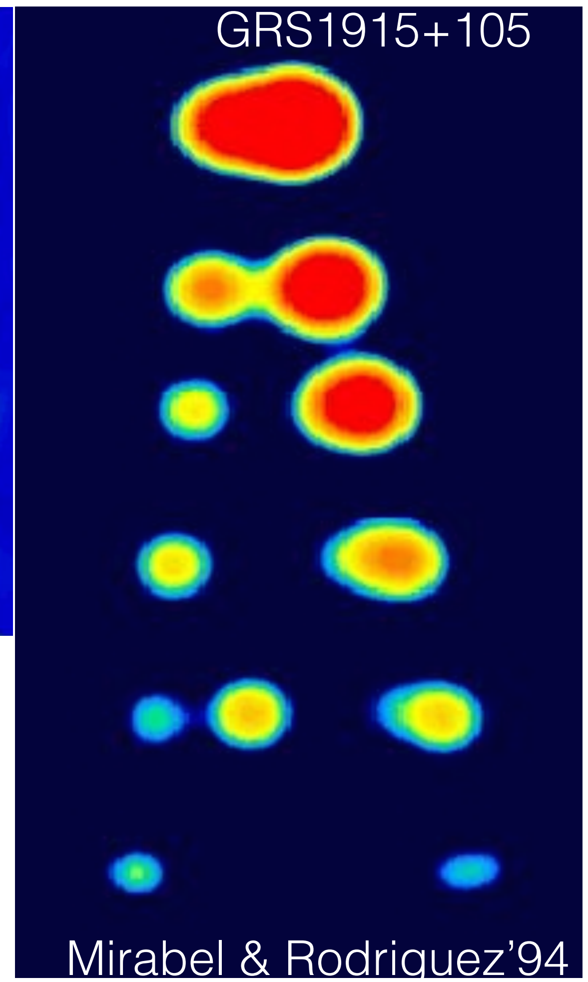

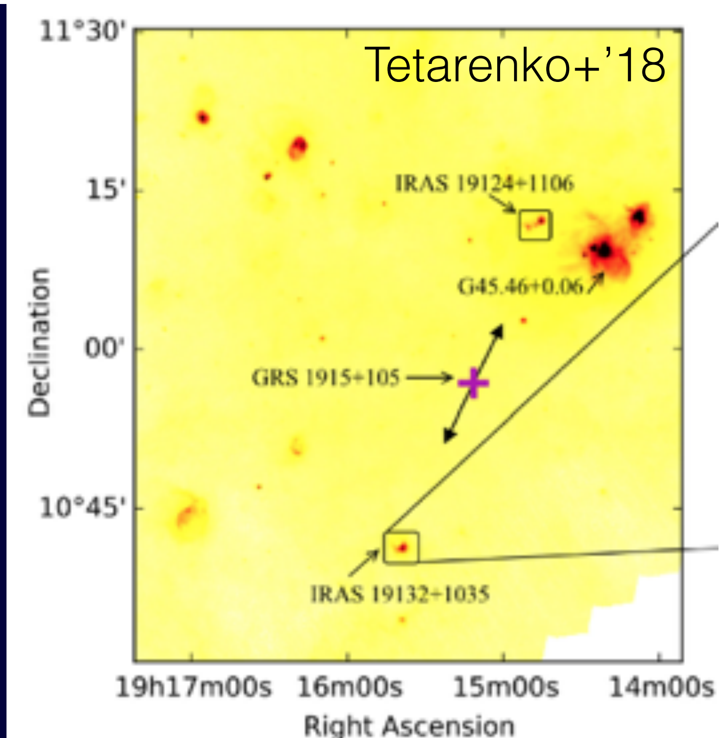

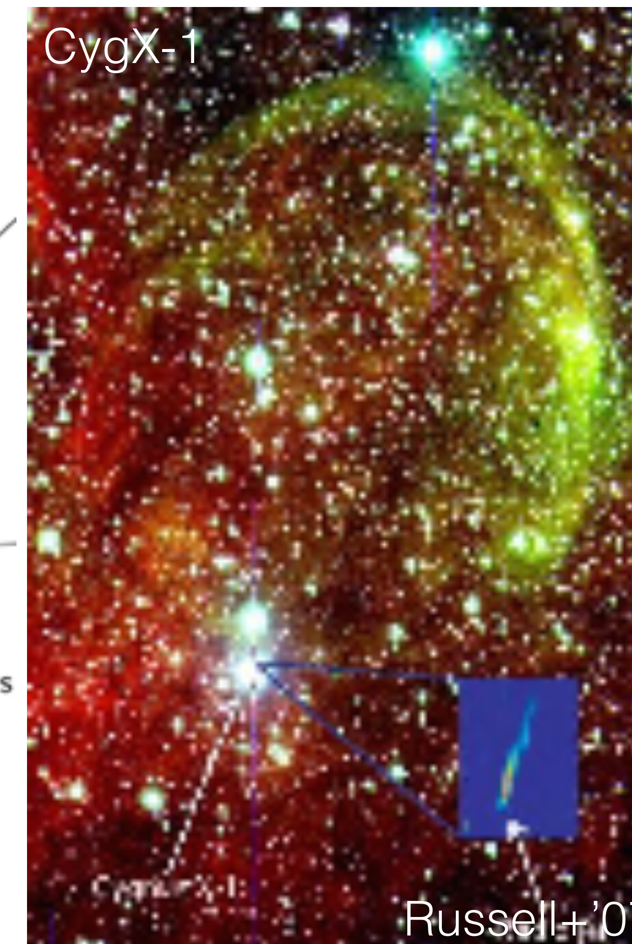

milli-arcsec

arcsec

arcmin -> degree

accretion & ejection relation

jet power & radio duty cycle interaction with the ISM

Jets through the BH mass scale

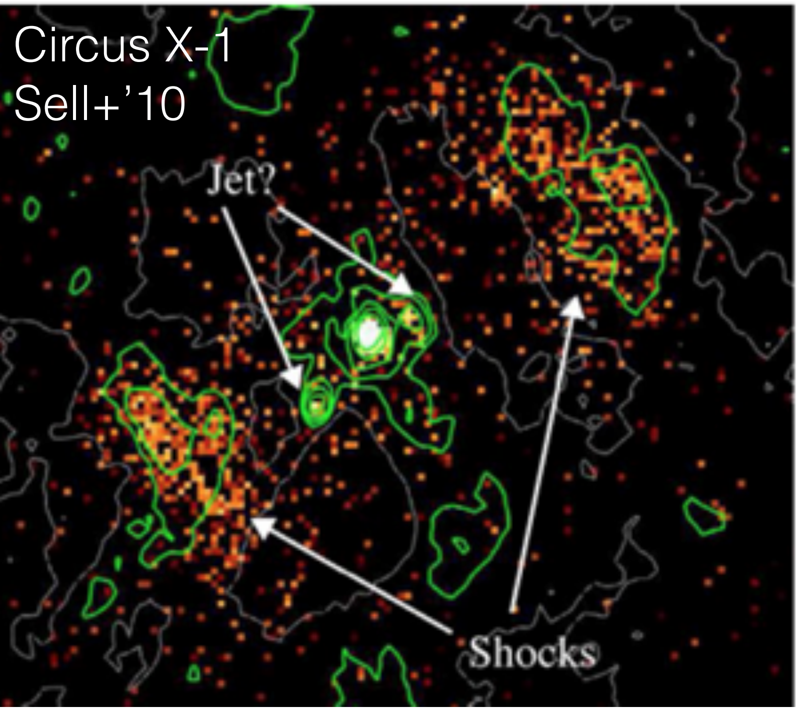

l_{jet}~0.5 pc jets in 10 M_{sun} BH

$r_g=2M_{BH}G/c^2$

l_{jet}/r_g

l_{jet}~5-50 Mpc jets in 10^{8-9} M_{sun} BH

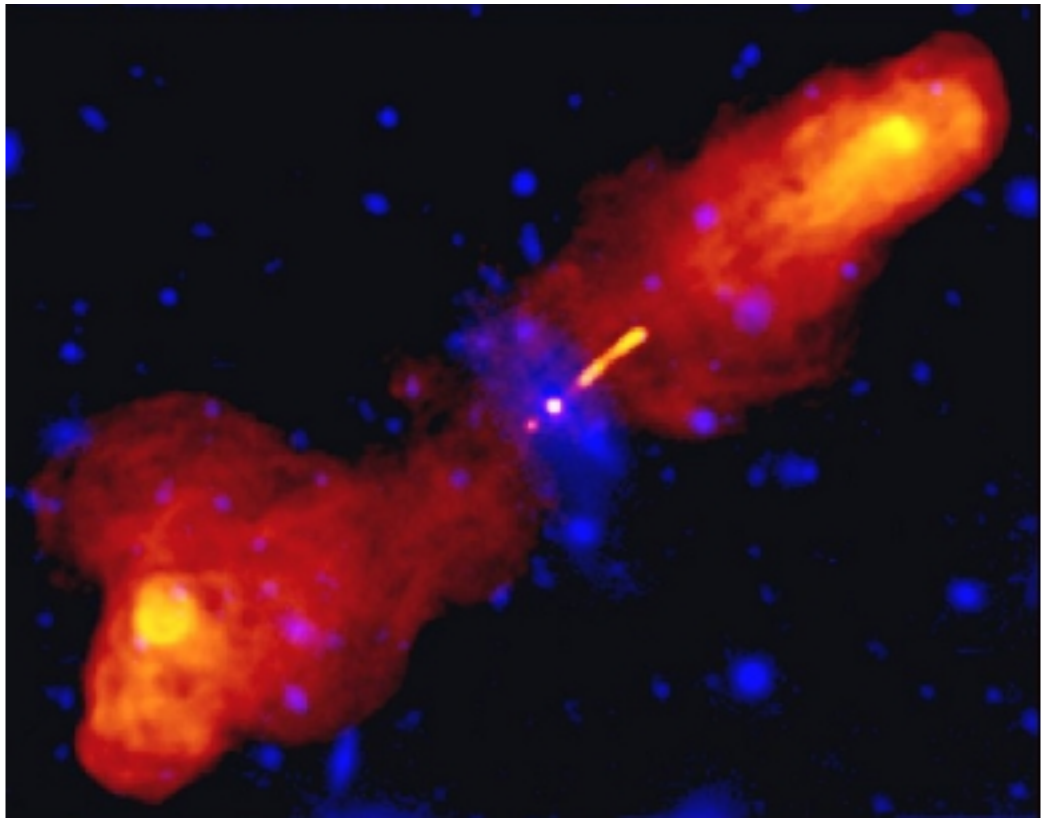

as observing Mpc jets of a radio galaxy moving, varying and changing morphology!(*)

(*: jet's thrust ratio is not the same, Heinz+2013)

A Galactic perspective: (micro)quasar large-scale X-ray jets

Giulia Migliori (DIFA, INAF-IRA)

S.Corbel, J. Tomsick, P. Kaaret, R. Fender, T. Tzioumis, M. Coriat, J. Orosz

XTE J1550-564 large scale jets

Low Mass X-ray Binary:

- BH mass: 9.1+/-0.6 M_{sun} (Orosz+'11);
- distance: 4.4+/-0.6 kpc;
- inclination: 75+/-4 degree;
- September 1998: X-ray outburst followed by the detection of relativistic compact jets (v_{app}~1.7c, Hannikainen+09);

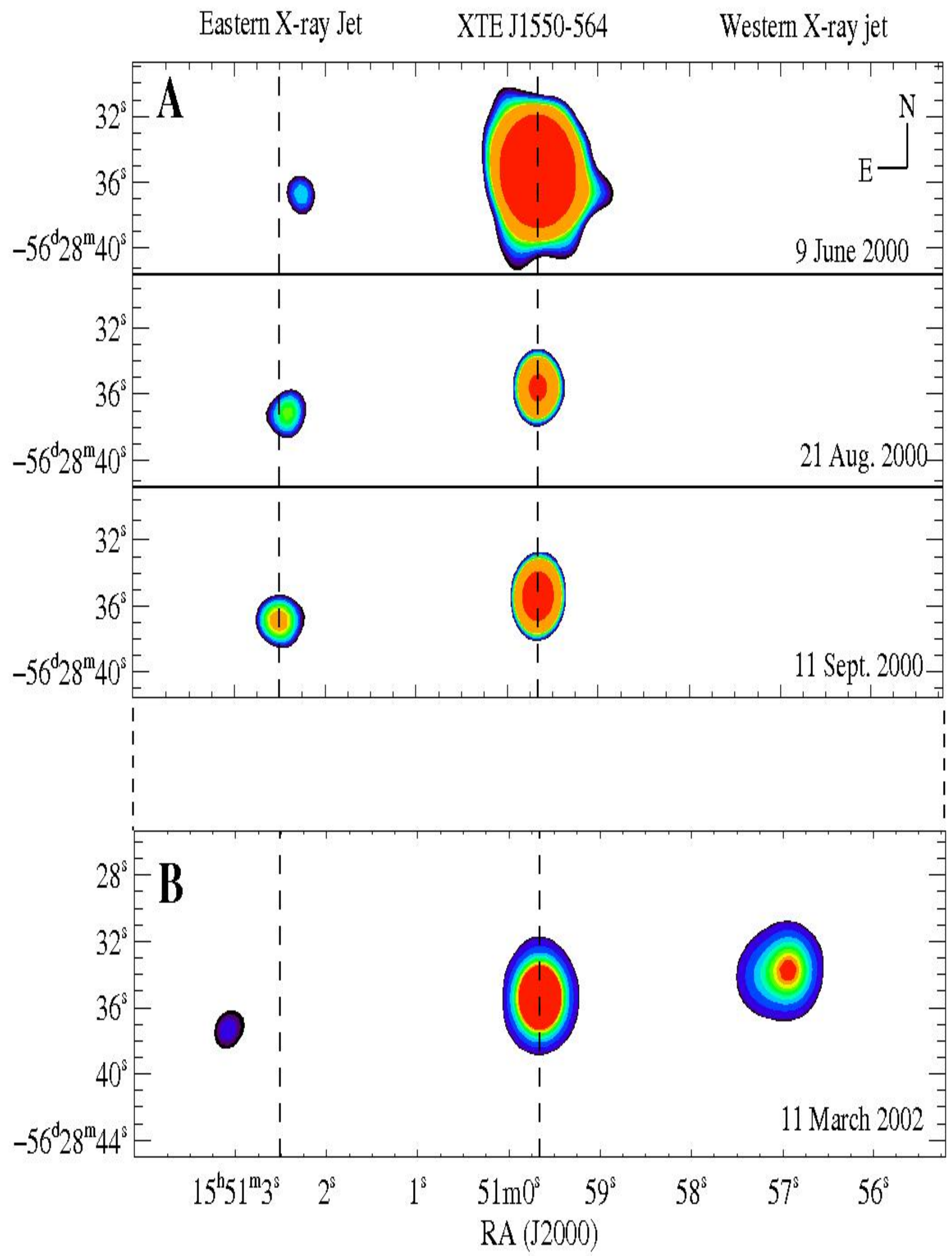

Corbel+'02

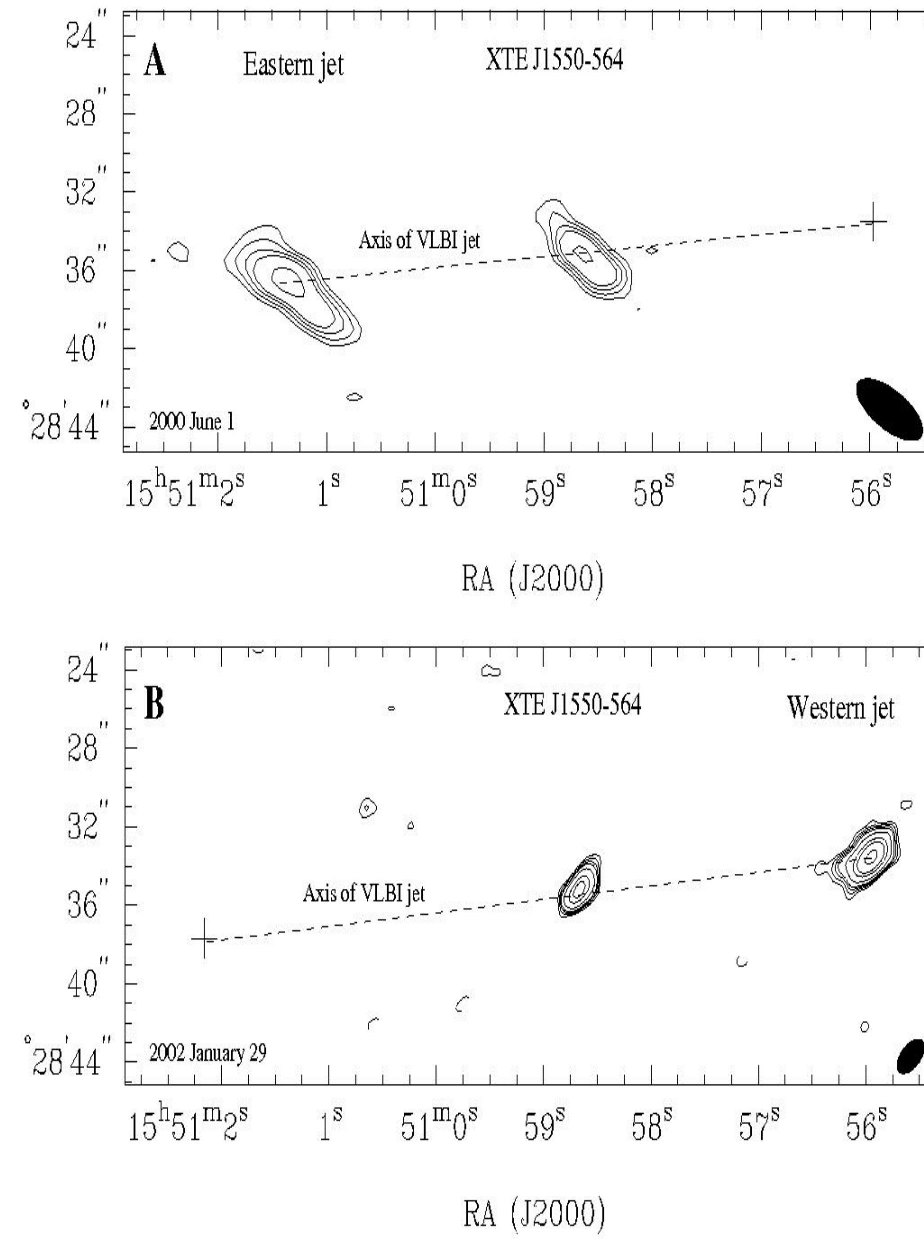

Discovery of large scale (~0.5pc) decelerating jets following the 1998 outburst

XTE J1550-564 large scale jets

Dynamical Model:

the jets propagate unseen in an under-dense ISM cavity and become visible when they impact the cavity's boundaries (Wang '03; Hao&Zhang '09, Steiner+'12).

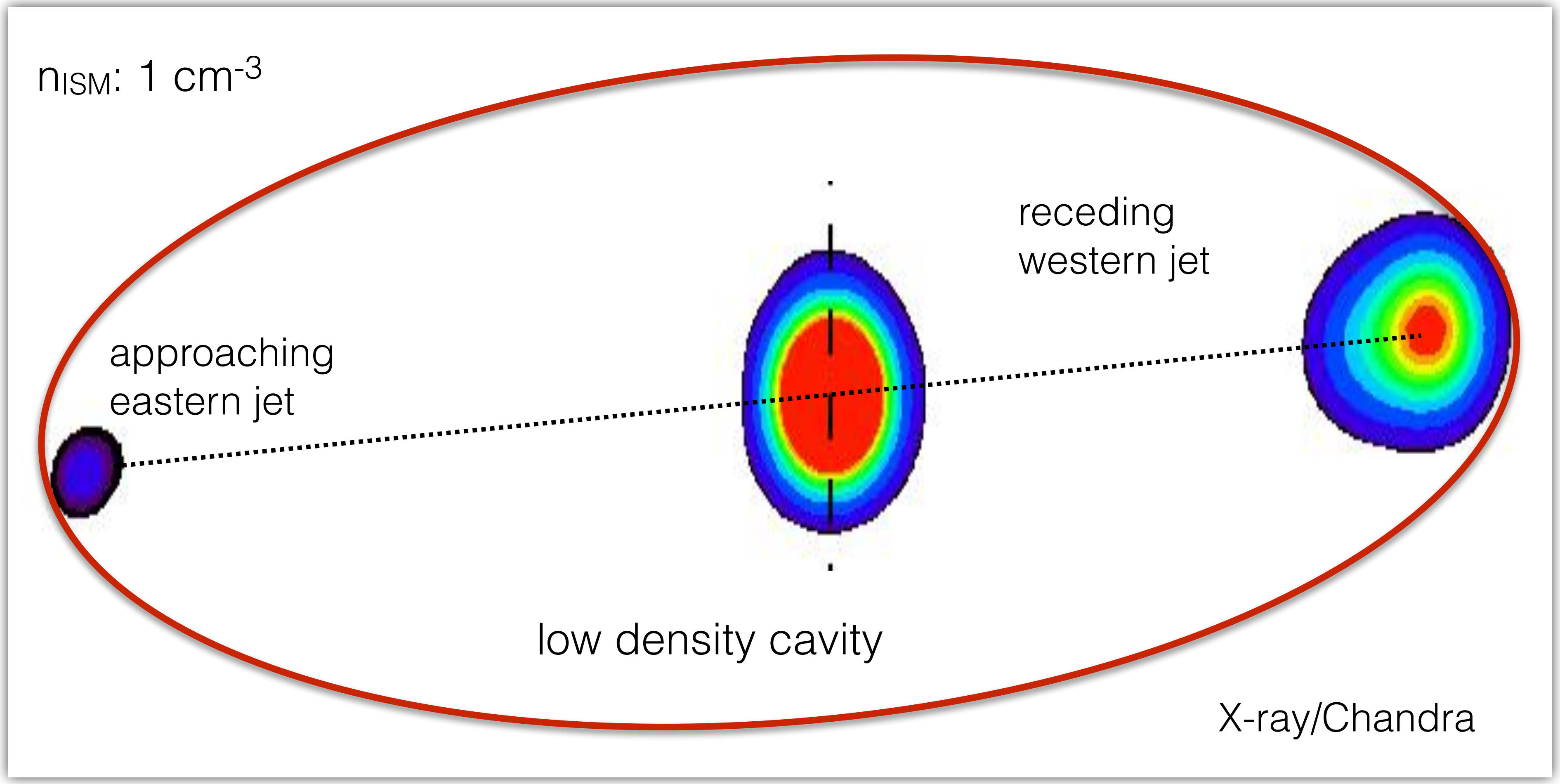

✓ X-ray follow-up: 8 Chandra observations;

★ Radio follow-up: 24 ATCA observations at 4 frequencies (1.4 GHz, 2.5 GHz, 4.8 GHz, 8.6 GHz).

Jets' dynamics

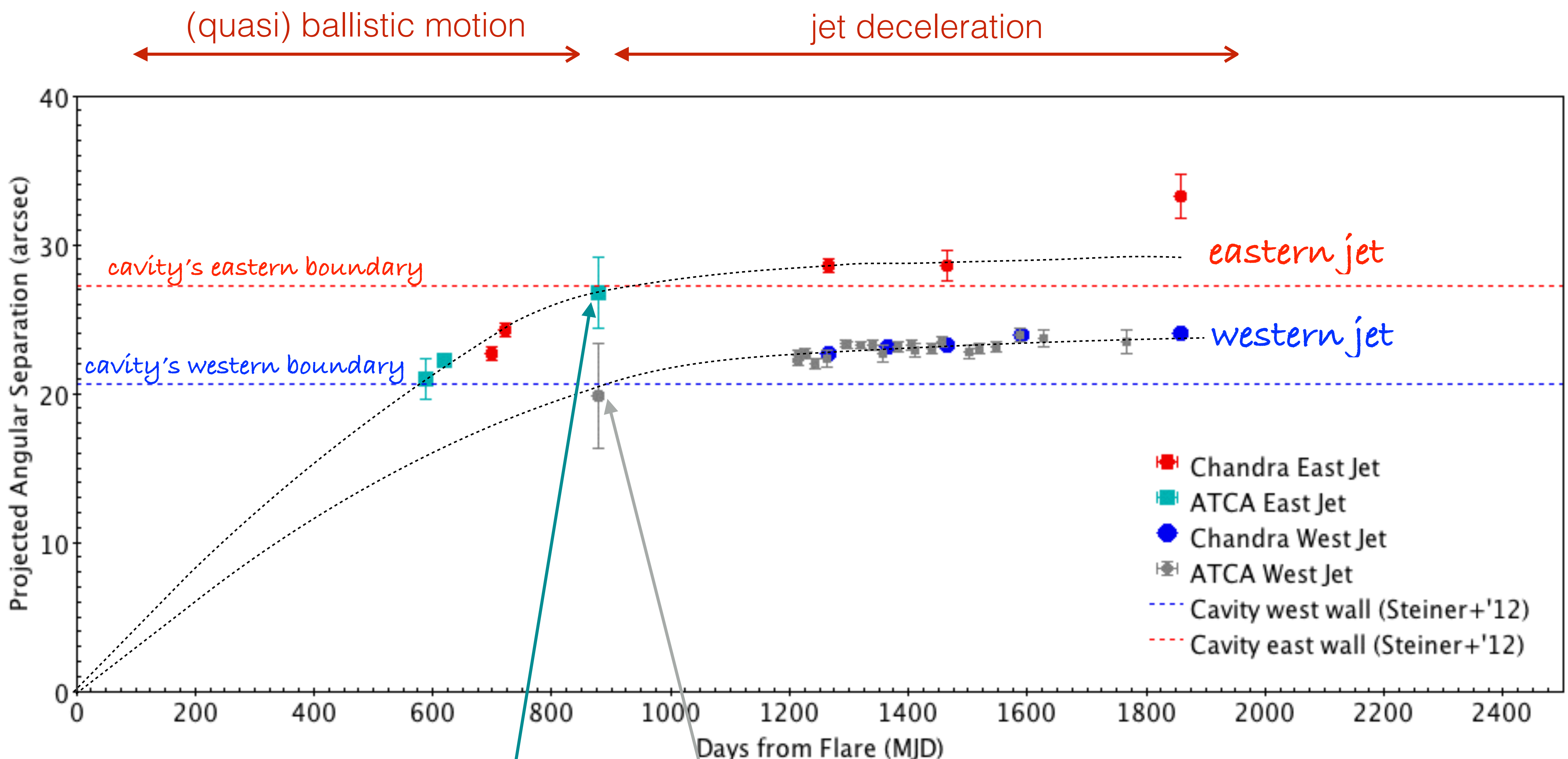

first detection of the western jet in 2001

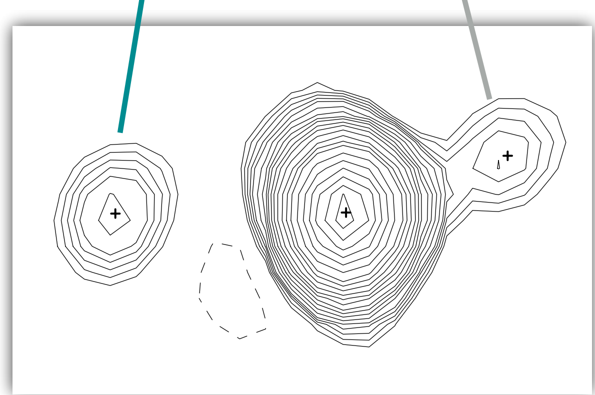

beginning of the deceleration phase

$\langle v_{app,eastjet} \rangle = 1.0c$ to $0.1c$;

$\langle v_{app,westjet} \rangle = 0.55c$ to $0.4c$.

Western Jet: X-ray morphology

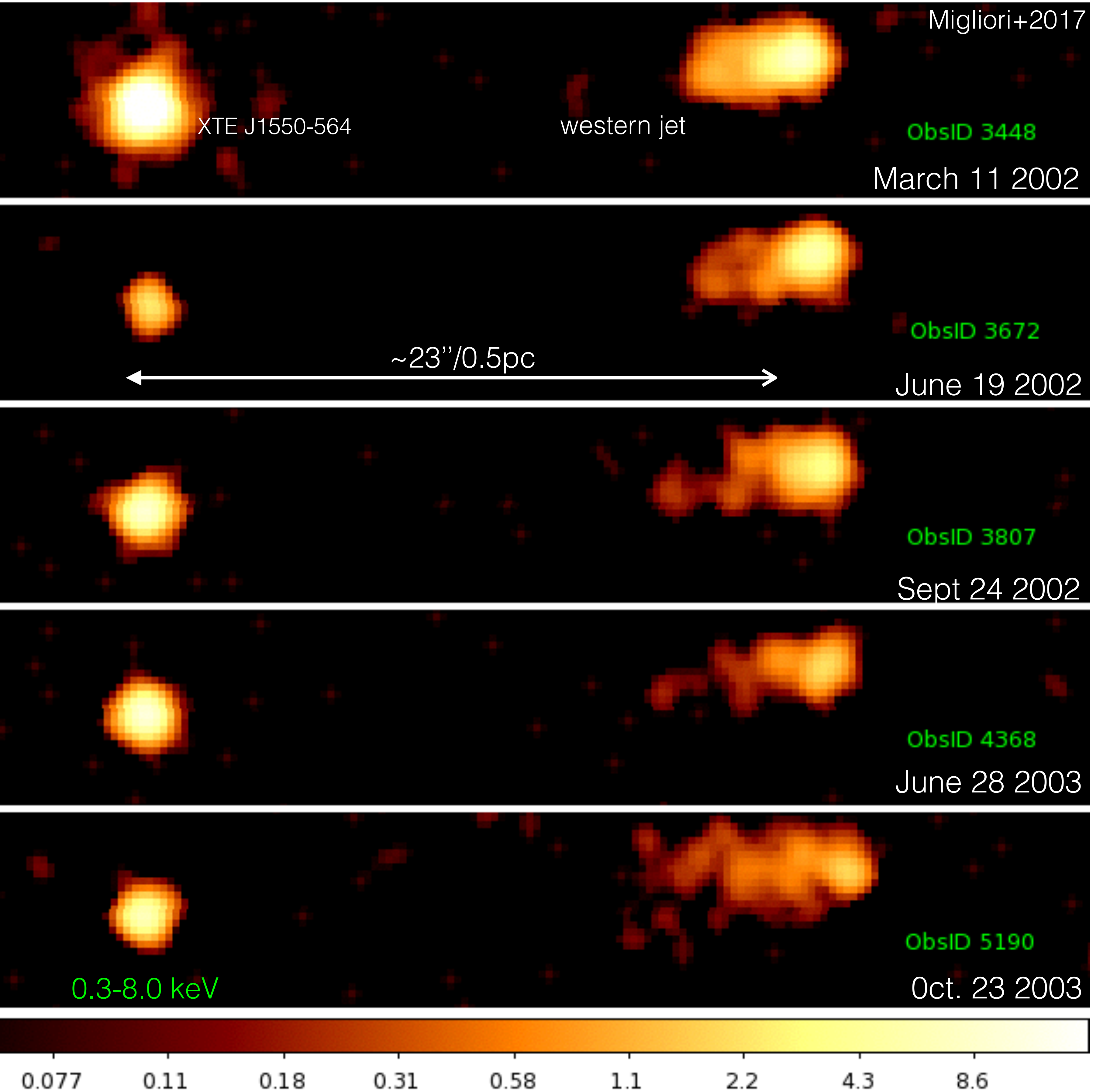

Spatially resolved, evolving X-ray morphology

Western Jet morphology

helical X-ray morphology?

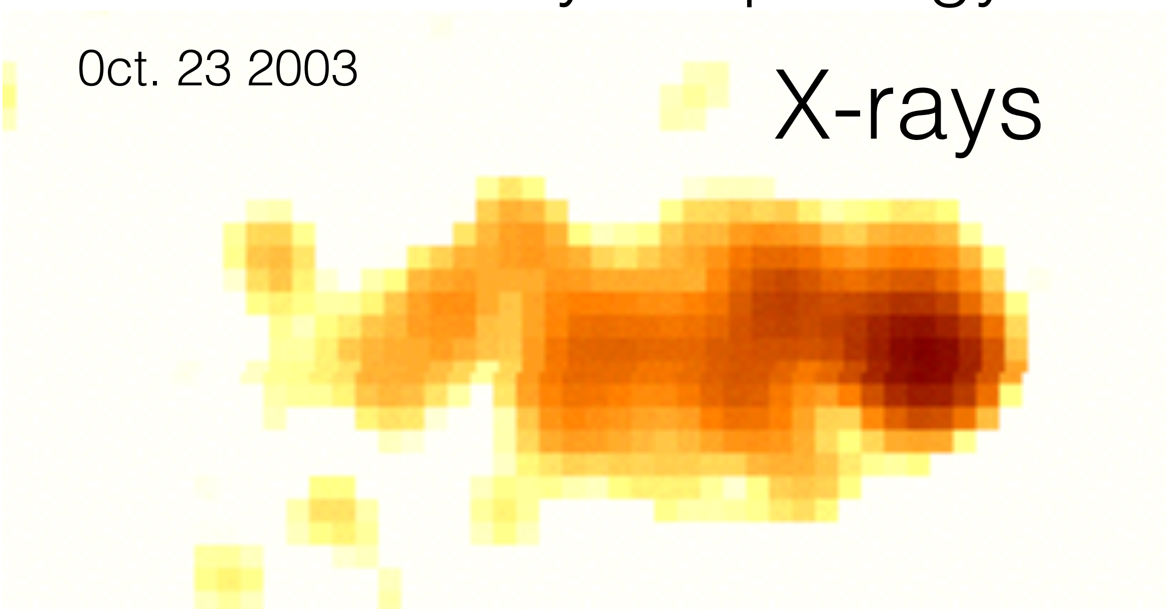

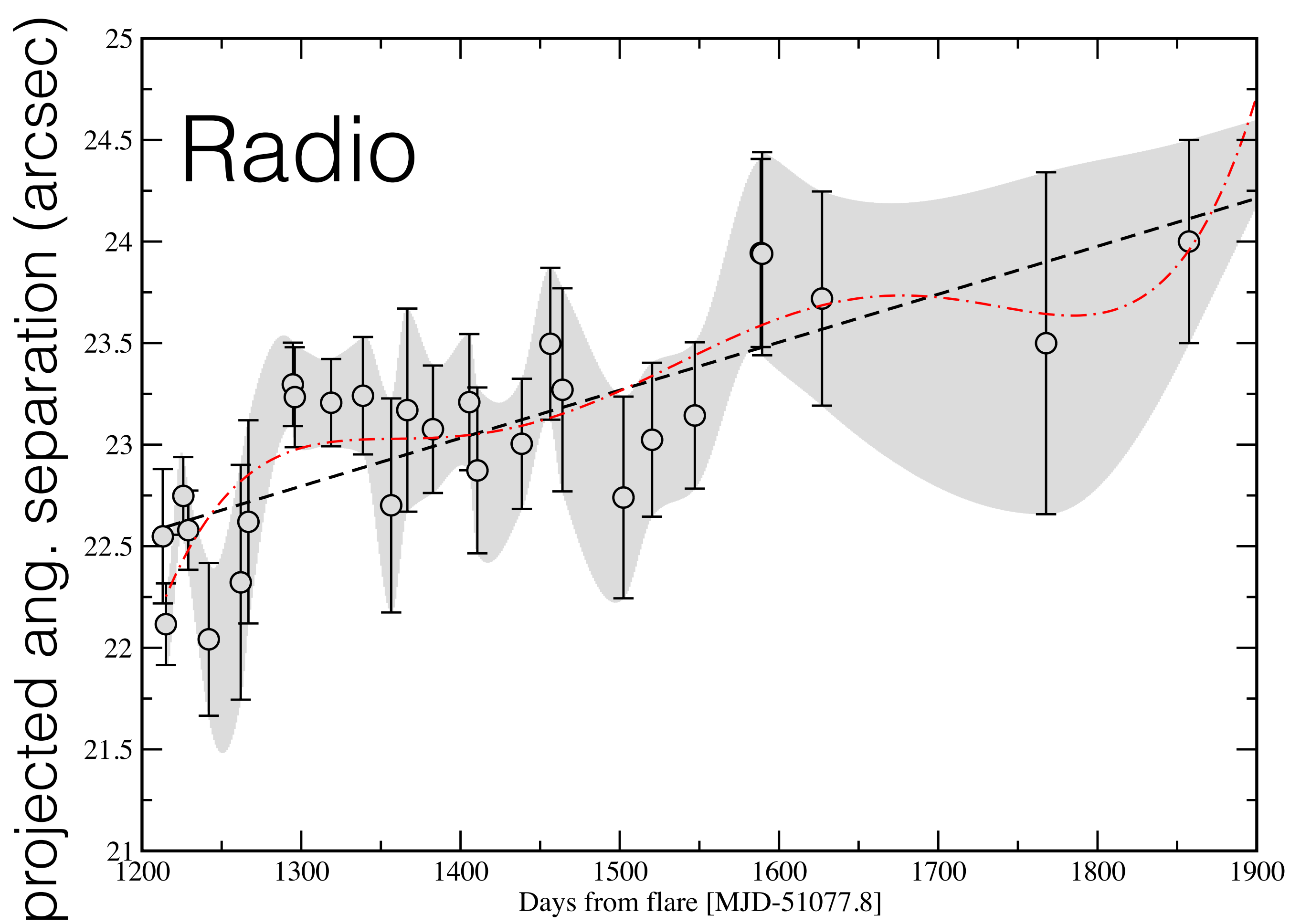

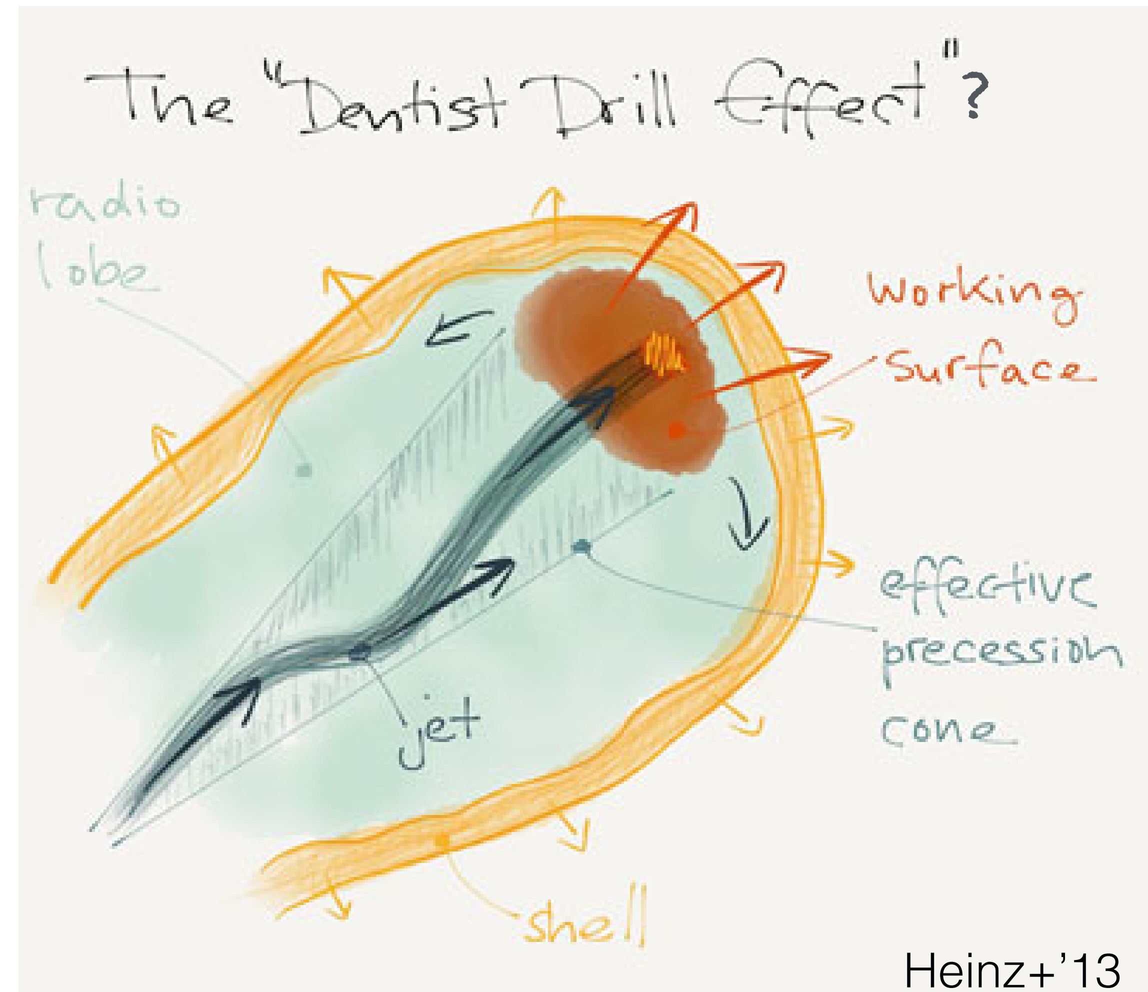

Western Jet: X-ray profiles

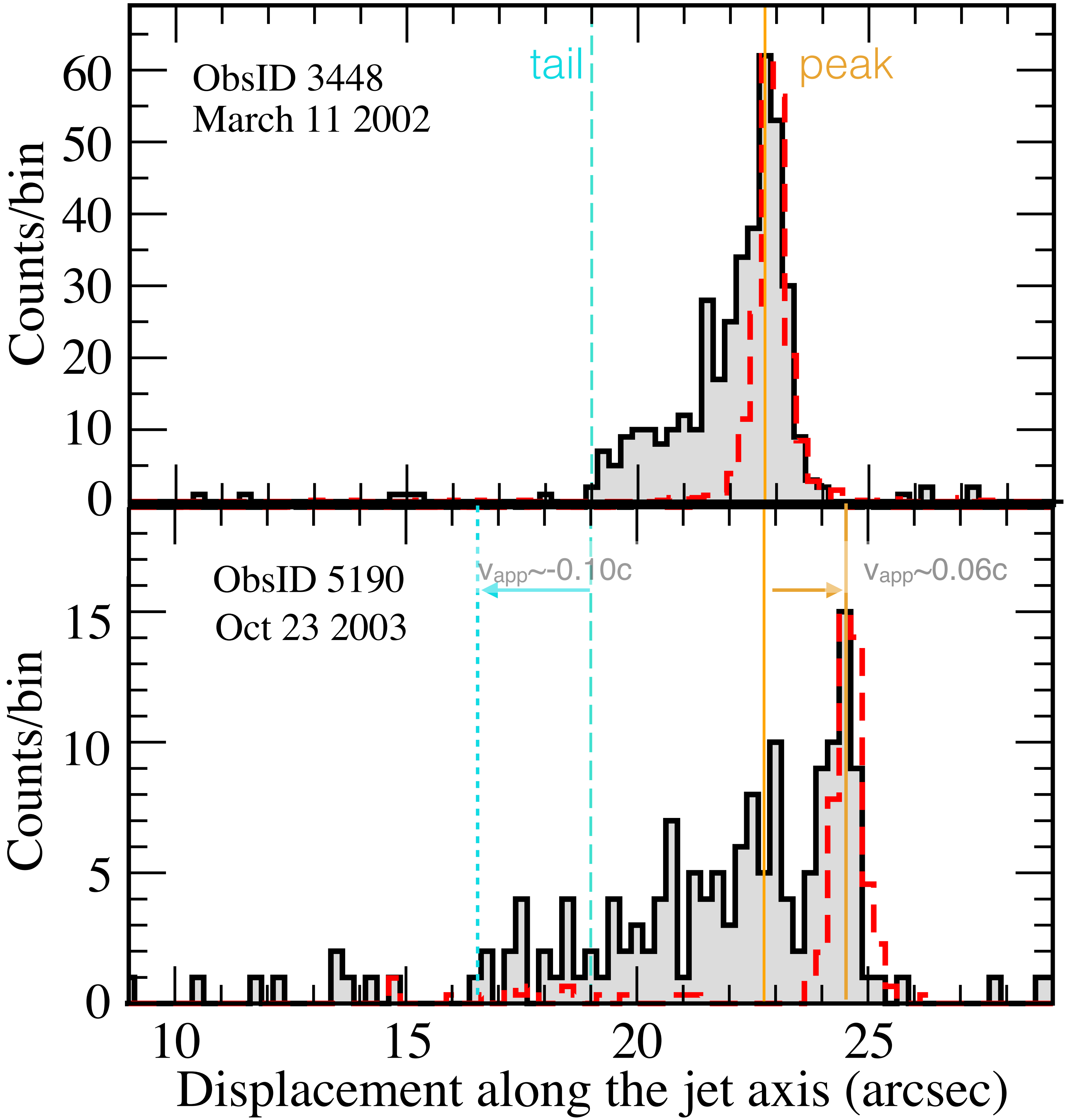

- progressive deceleration of the main peak (v_{app}~0.06c);
- formation of an apparently receding tail (v_{app}~-0.10c);

X-ray emission decay

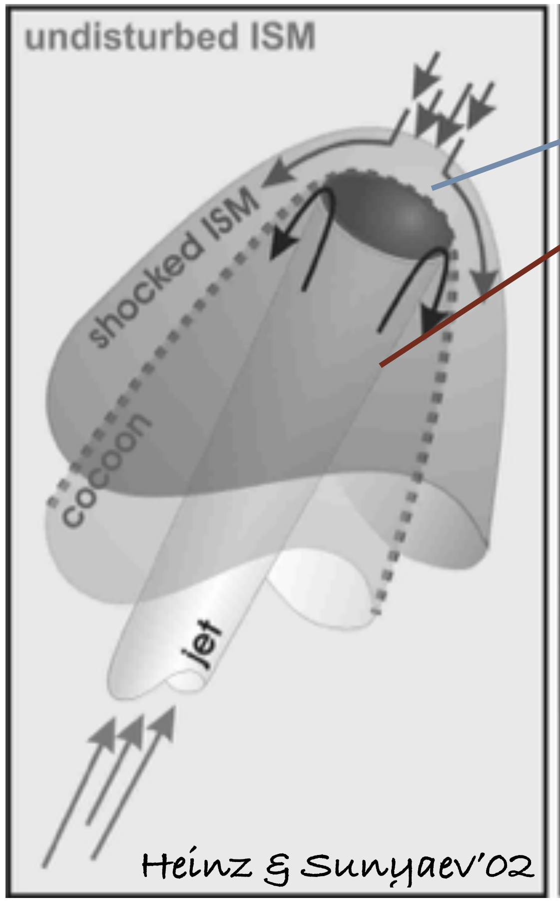

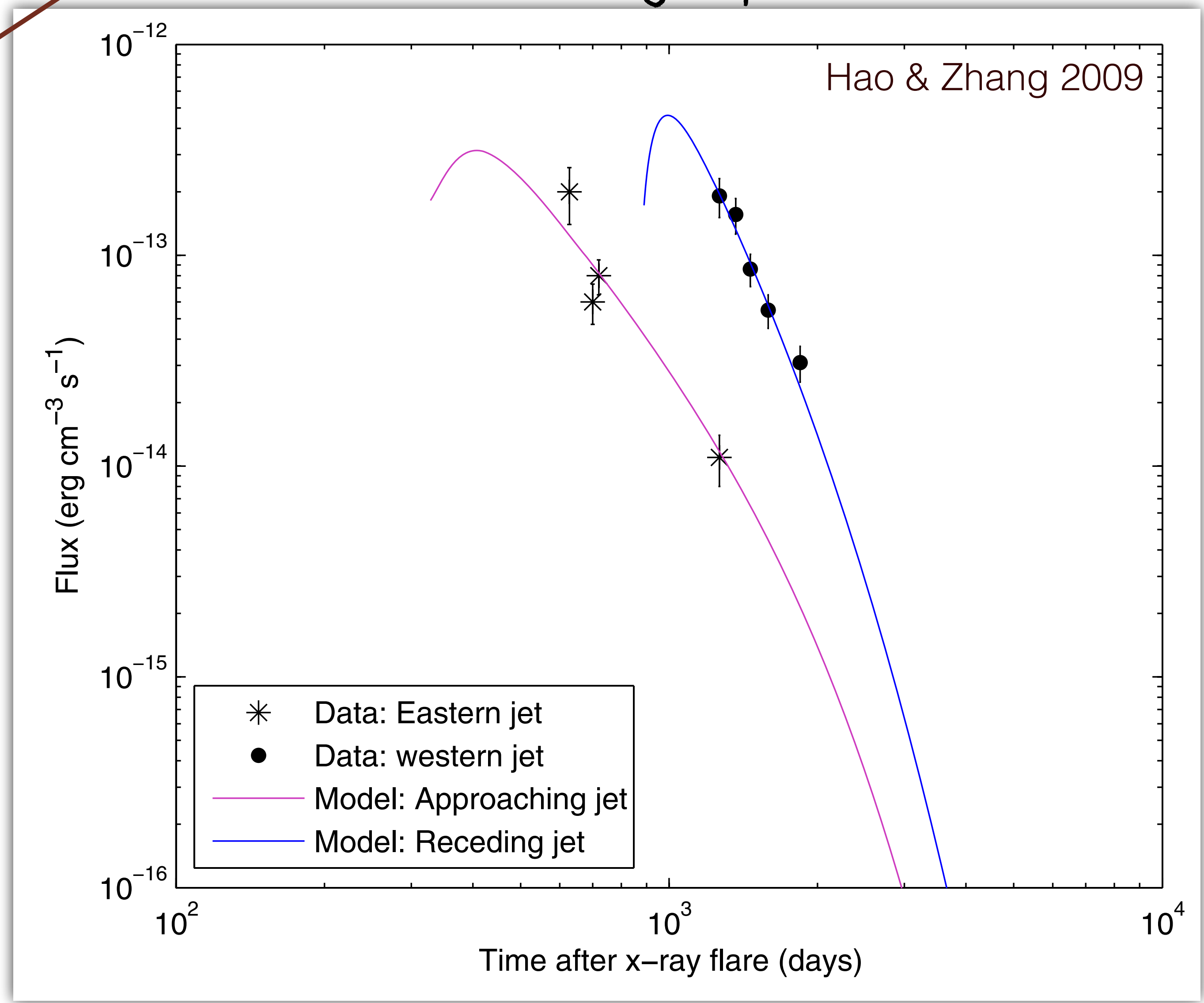

<u>Radiative Model</u>:

- radiating particles accelerated by the reverse shock (Wang 2003; Hao & Zhang 2009);
- X-ray from synchrotron mechanism;
- energy losses dominated by adiabatic expansion losses.

Radio-X-ray SED

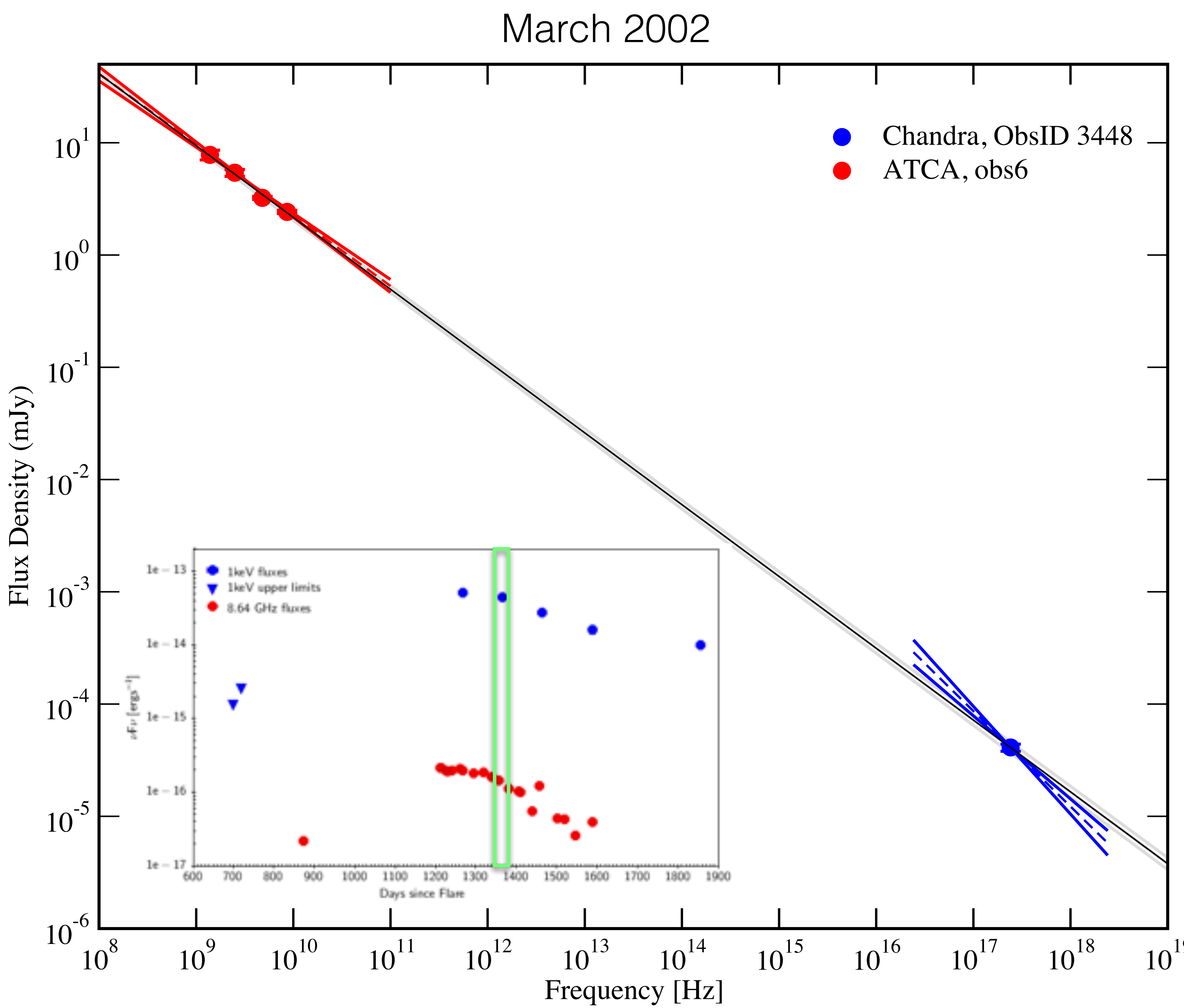

SED consistent with radio-X-ray synchrotron emission:

B_{eq}~0.2-0.1 mG, E_{min}~10^{42} erg, P_{jet}~10^{37} erg/s

Western jet: X-ray & radio light curves

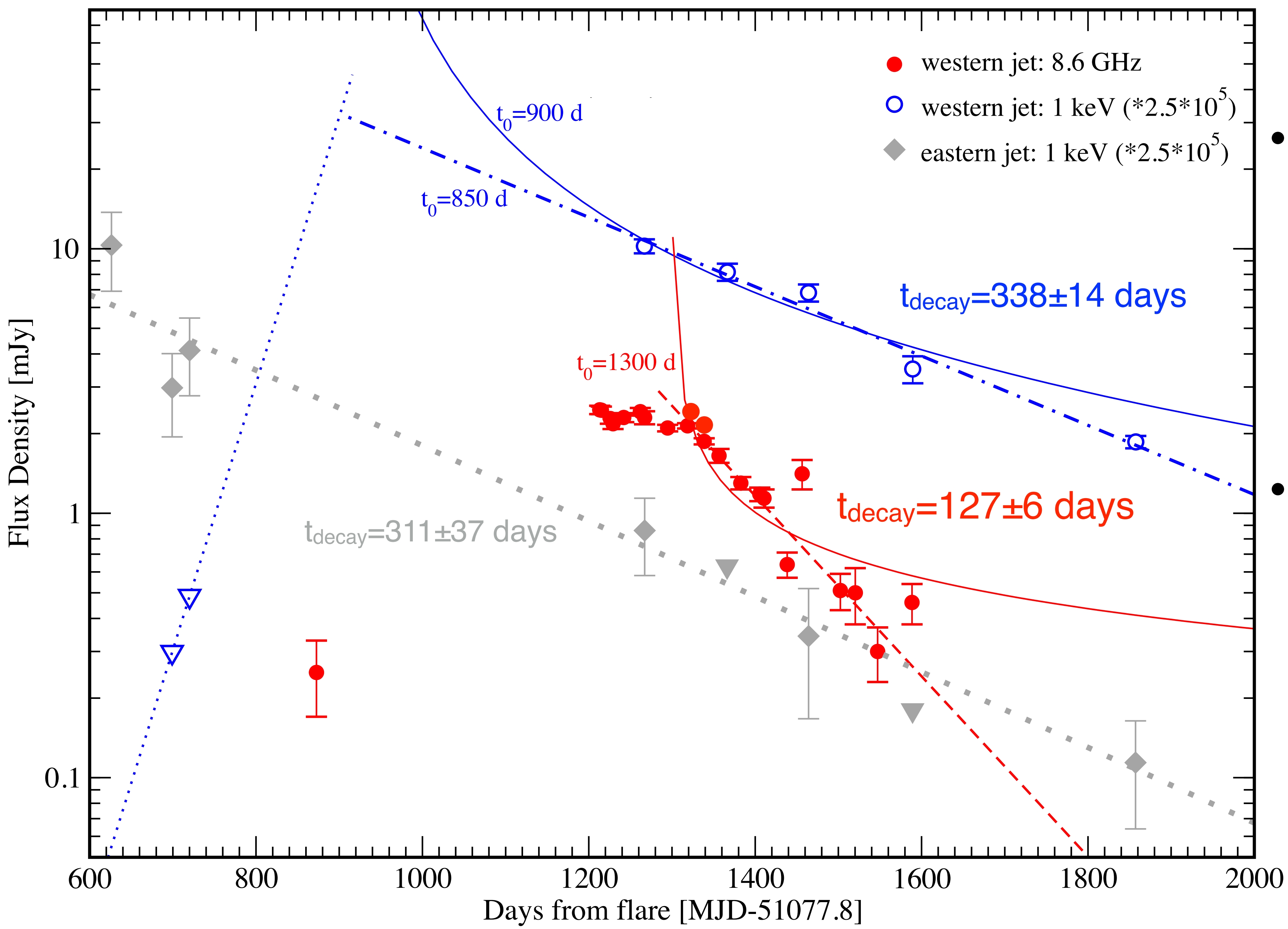

- steep (~2.0) power-law decay consistent with a reverse shock operating only once on the jet plasma (Wang'03, Genet, Daigne & Mochkovitch 2007,Hao & Zhang '09)
- **Chromatic decay:** faster decay of the emission in radio than in X-rays (same for the jets of H1743-322, Corbel+'05)

Not consistent with dominant adiabatic or radiative losses

Radio-X-ray SED

September 2002

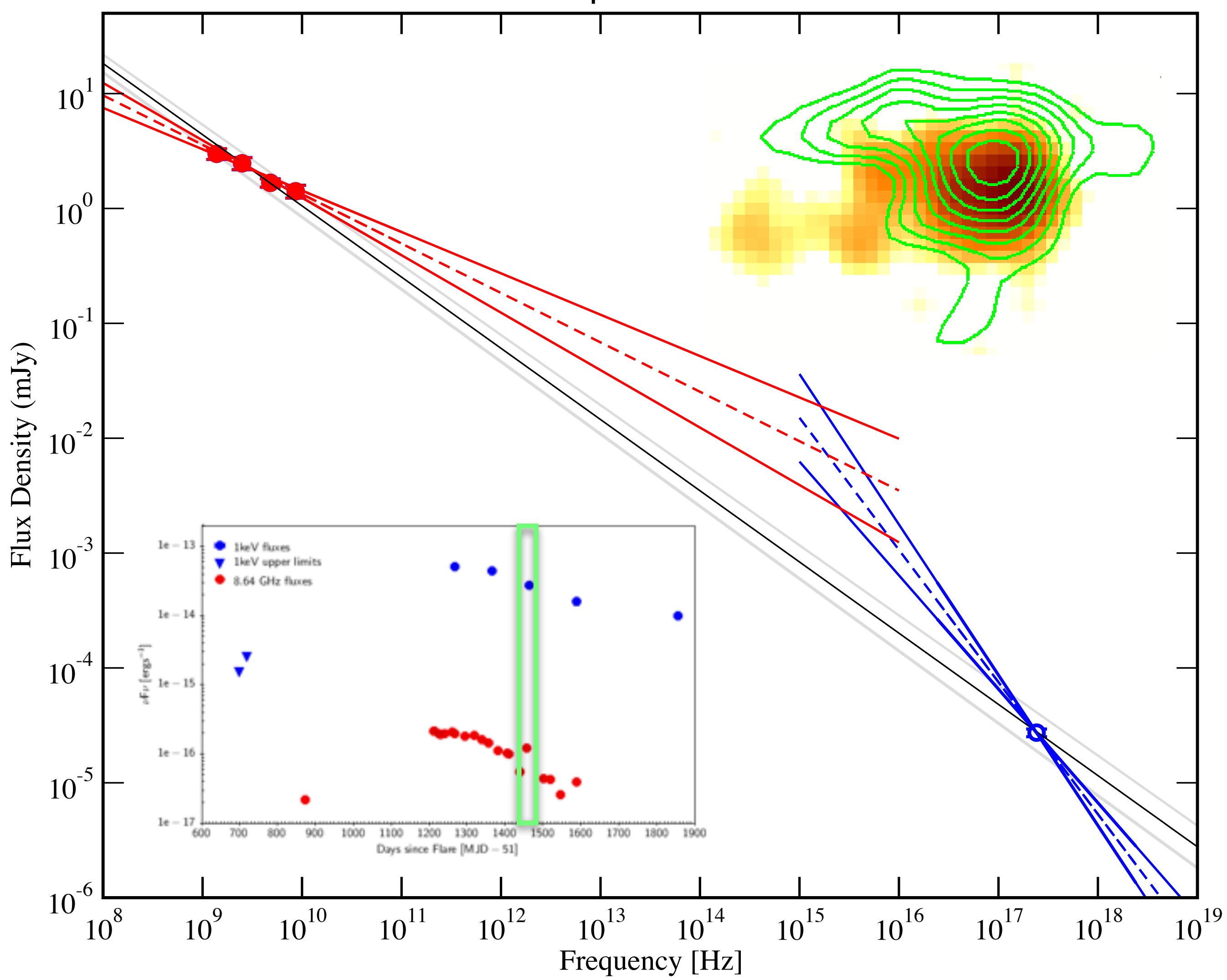

FRII hot spots:

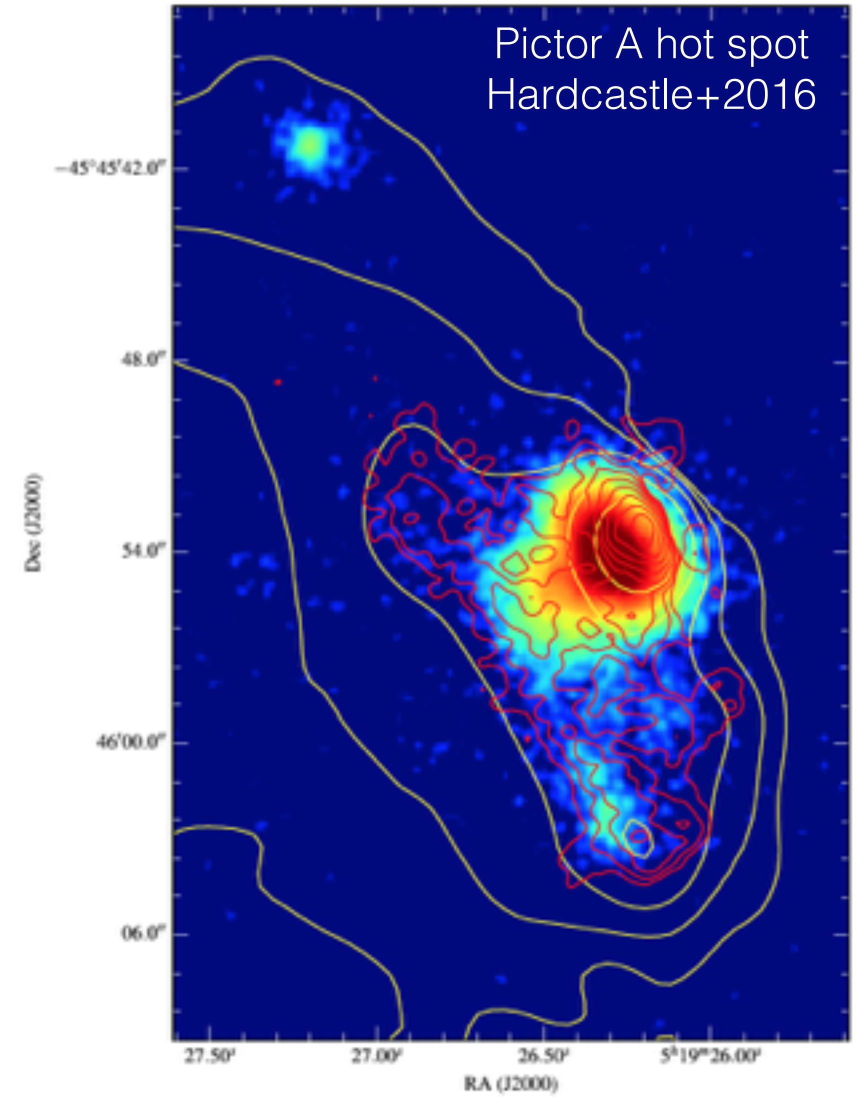

- evidence of spectral changes at the time of a radio flare
- flattening of the radio spectrum + break @10^{15} Hz;
- different radio and X-ray morphologies & peak offsets?

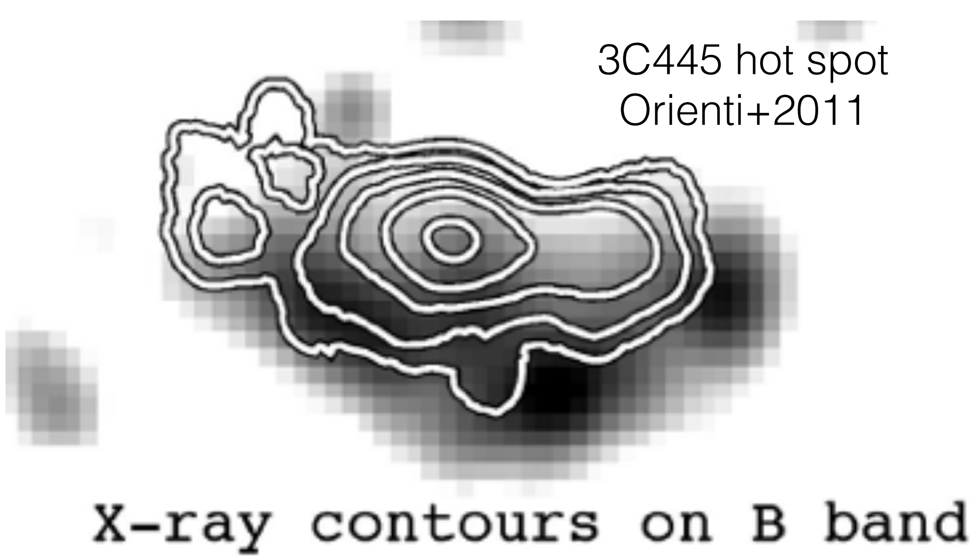

X-ray Tail: colliding shells

Emission produced by internal shocks formed by colliding plasma shells

compact jets of microquasars, prompt emission of GRBs, blazars (Kaiser+'00, Jamil+'10, Malzac+'14,Sari&Piran'97,Spada+'01)

AGNs: colliding plasma knots in the kpc jet of the radio galaxy 3C 264

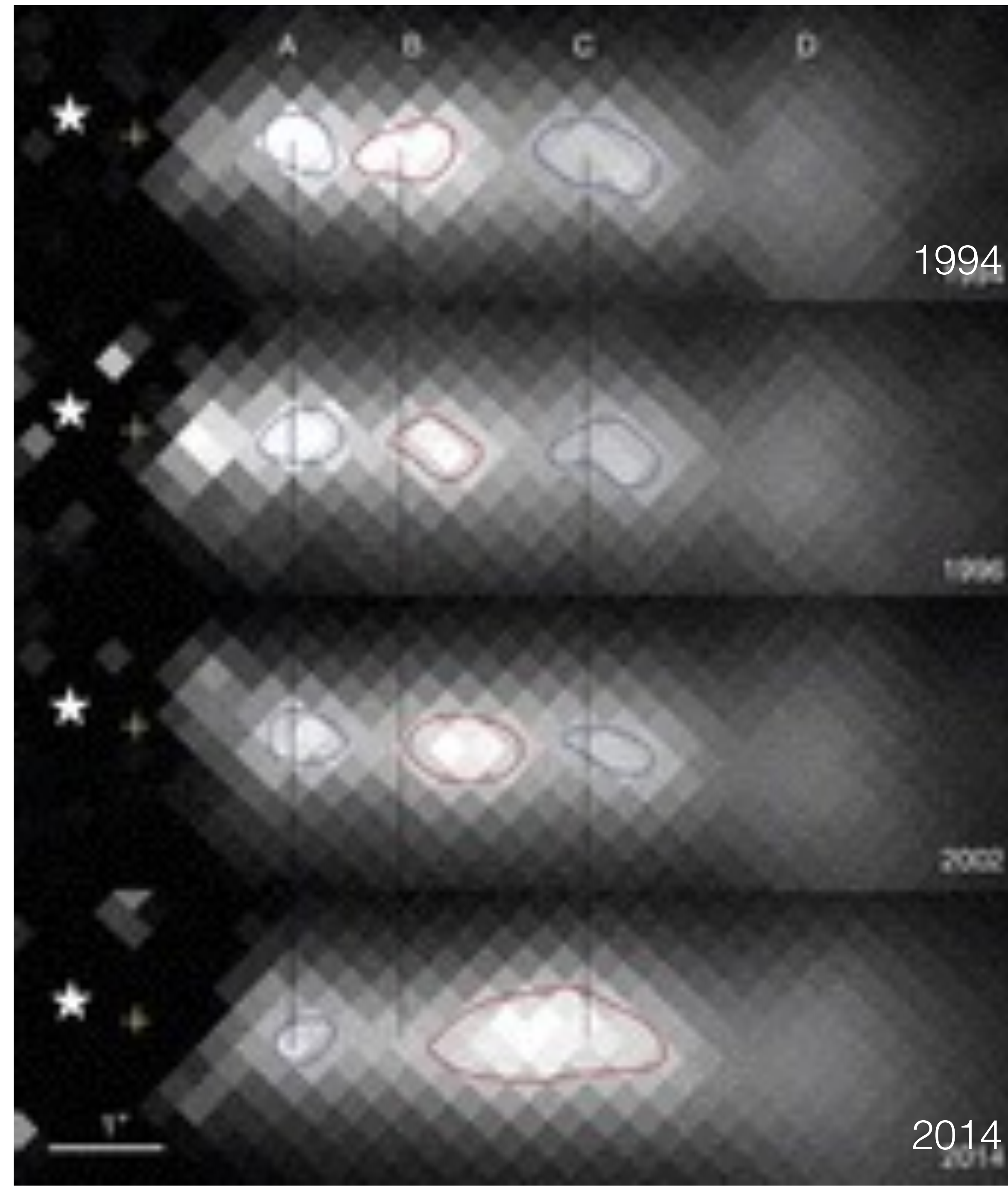

Meyer+'15

Polarized radio emission

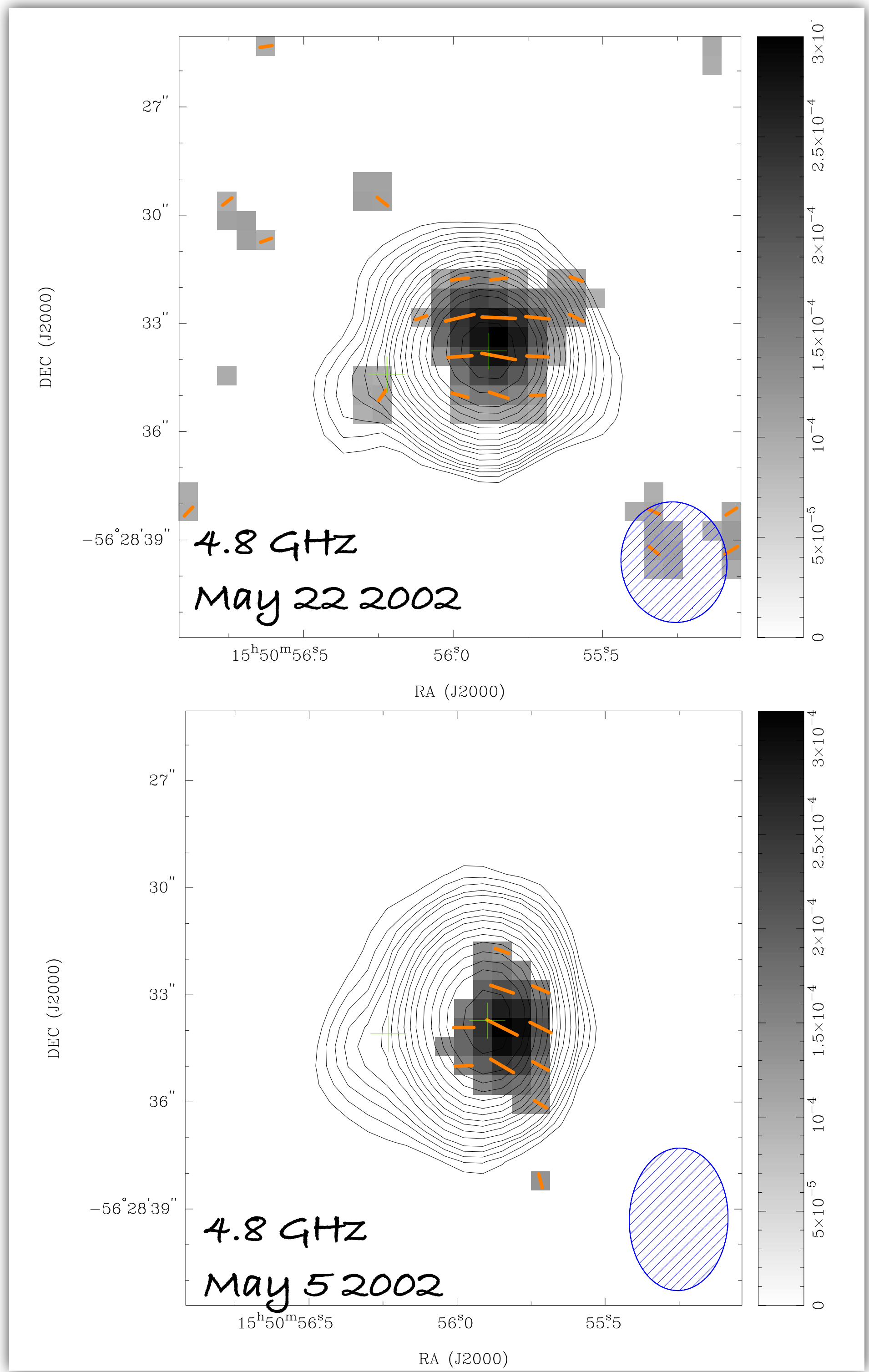

- up to 9% linearly polarized flux @4.8 GHz and 8.6 GHz;
- E vector parallel to the jet axis;
- polarization angle changes on <month timescales.

shock-compressed B field
+
evolution of the jet internal structure

FRII hot spots:

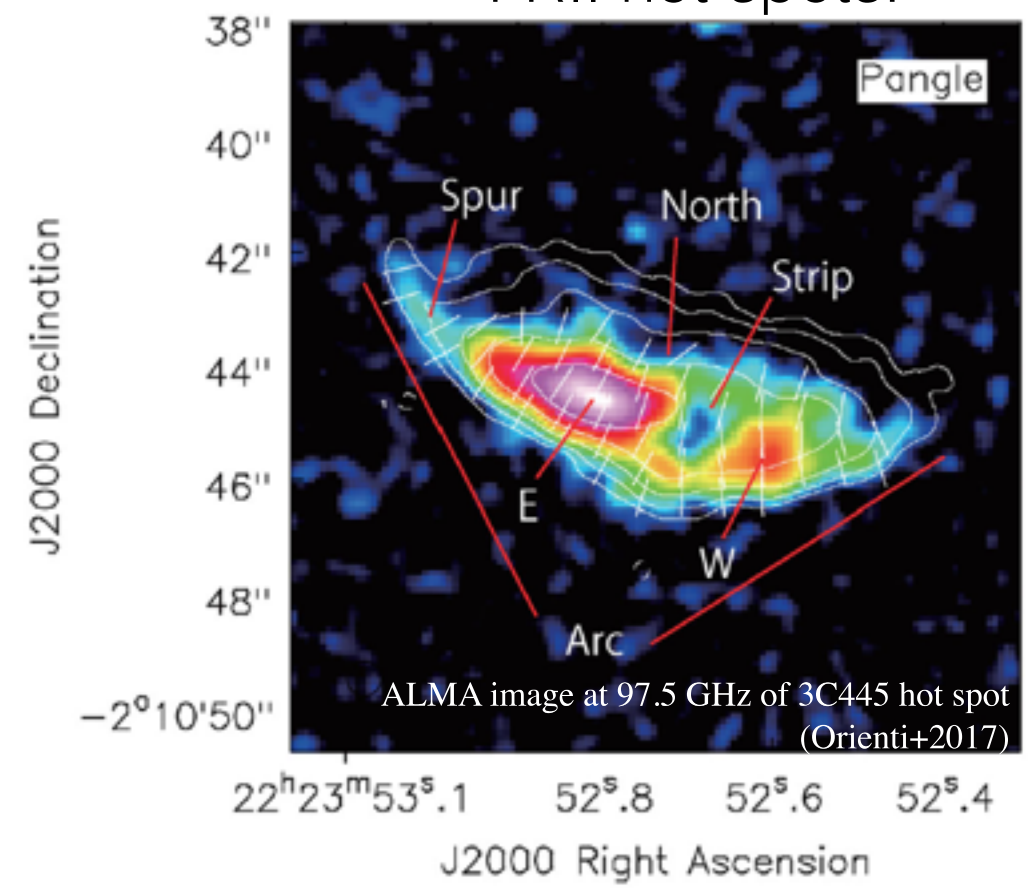

ALMA image at 97.5 GHz of 3C445 hot spot (Orienti+2017)

Conclusions

Radio & X-ray monitoring of the large scale jets of XTE J1550-564 unveiled jet-ISM and particle acceleration in action.

For now we need intense/time-expensive monitoring to discover these jets but..
future facilities (SKA, LSST…) will allow systematic studies.

Microquasars can help us understand many aspects of the radio activity of BH.

Western jet: X-ray & radio light curves

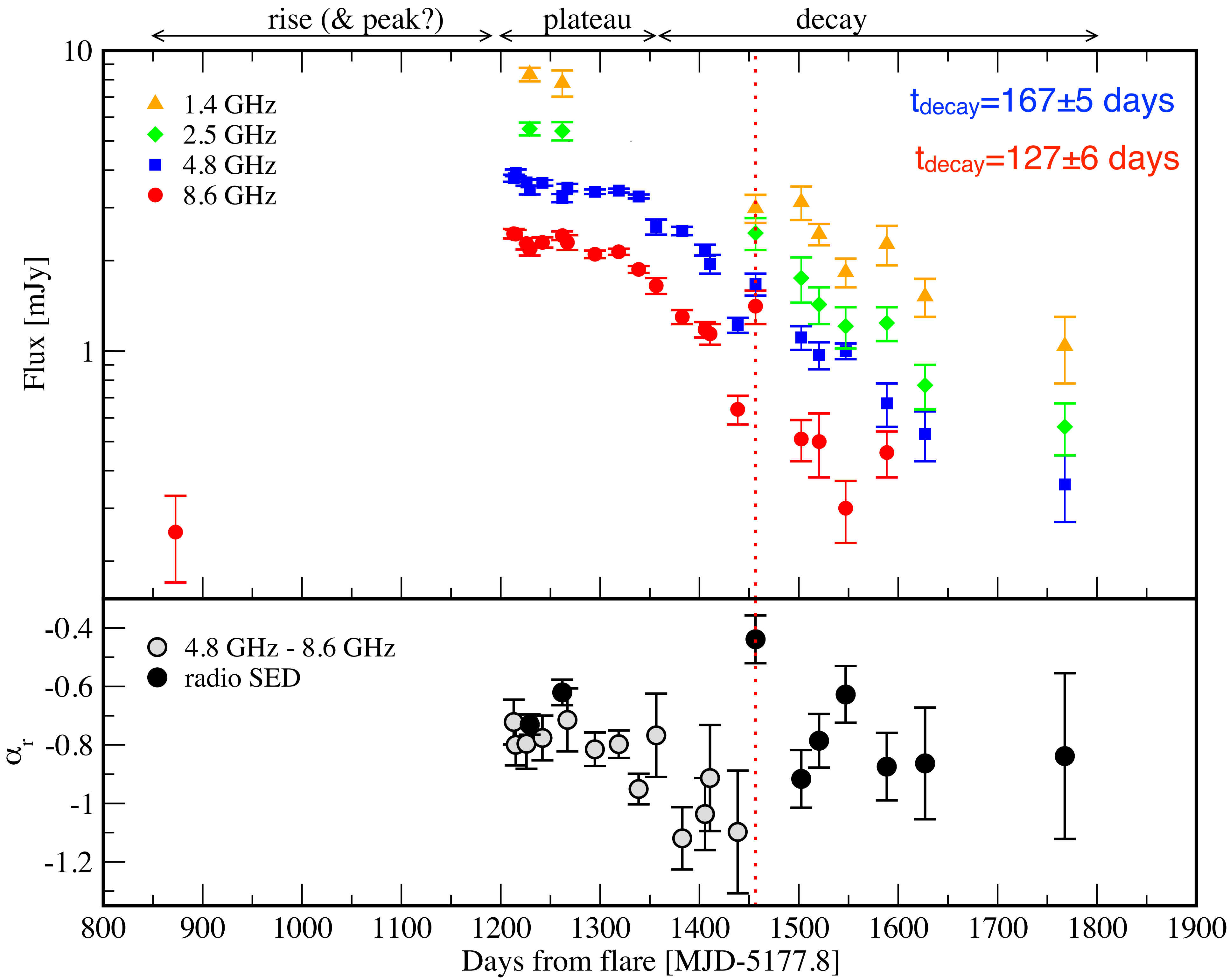

@8.6 GHz: flux re-brightening + spectral flattening in September 2002

newly accelerated low-energy particles?

From quasars to microquasars

Setting the stopping length in relation to the fundamental scale of the accreting system, given by the gravitational radius $r_g = GM/c^2$, defines one of the fundamental dimensionless numbers for jet dynamics (Heinz 2002), which we shall call the thrust ratio $\eta_{\rm jet}$:

$$\eta_{\rm jet} \equiv \frac{l_s}{r_g} = \frac{P^{1/2}}{\rho_{\rm ISM}^{1/2} M} \frac{c^{1/2}}{\pi^{1/2} G\theta_{\rm jet}} \propto \sqrt{\frac{1}{\rho_{\rm ISM} M}} \qquad (3)$$

where we may expect $\theta_{\rm jet}$ to be independent of black hole mass (though it may depend on accretion rate and spin).

Let us compare the thrust ratio for microquasars and typical radio galaxies. For microquasars, it is reasonable to assume ISM density of $n_{\rm ISM} \sim 1\ {\rm cm}^{-3}$, while the density in the intergalactic medium ranges from similar densities within the host galaxies of the AGN to $n_{\rm ISM} \sim 10^{-3}\ {\rm cm}^{-3}$ in clusters and lower densities yet in the environments of field galaxies. For representative black hole masses of $M_{\rm BH} \sim 10\ M_\odot$ and $M_{\rm BH} \sim 10^9\ M_\odot$ for microquasars and AGN jets, respectively, the thrust ratios for microquasars are much larger than those for AGN jets:

$$\eta_{\rm microquasar} \sim 10^3 \text{ to } 10^4 \eta_{\rm AGN} \qquad (4)$$

Thus, the ISM provides a much weaker barrier to microquasar jets than it does to AGN jets.

One important consequence of this is that the structures generated by the interaction of microquasar jets with the ISM will appear on observable scales on the sky, despite the fact that the angular scales of Galactic X-ray Binary (XRB) accretion disks on the sky are many orders of magnitude smaller than those of nearby AGN.

Another important consequence is that the surface brightness of the observational signatures of this interaction is generally low, i.e., signatures of microquasar–ISM interaction should generally be hard to detect. This is consistent with the fact that such signatures have only been found in a handful of sources.

Heinz+'13

Jets' dynamics

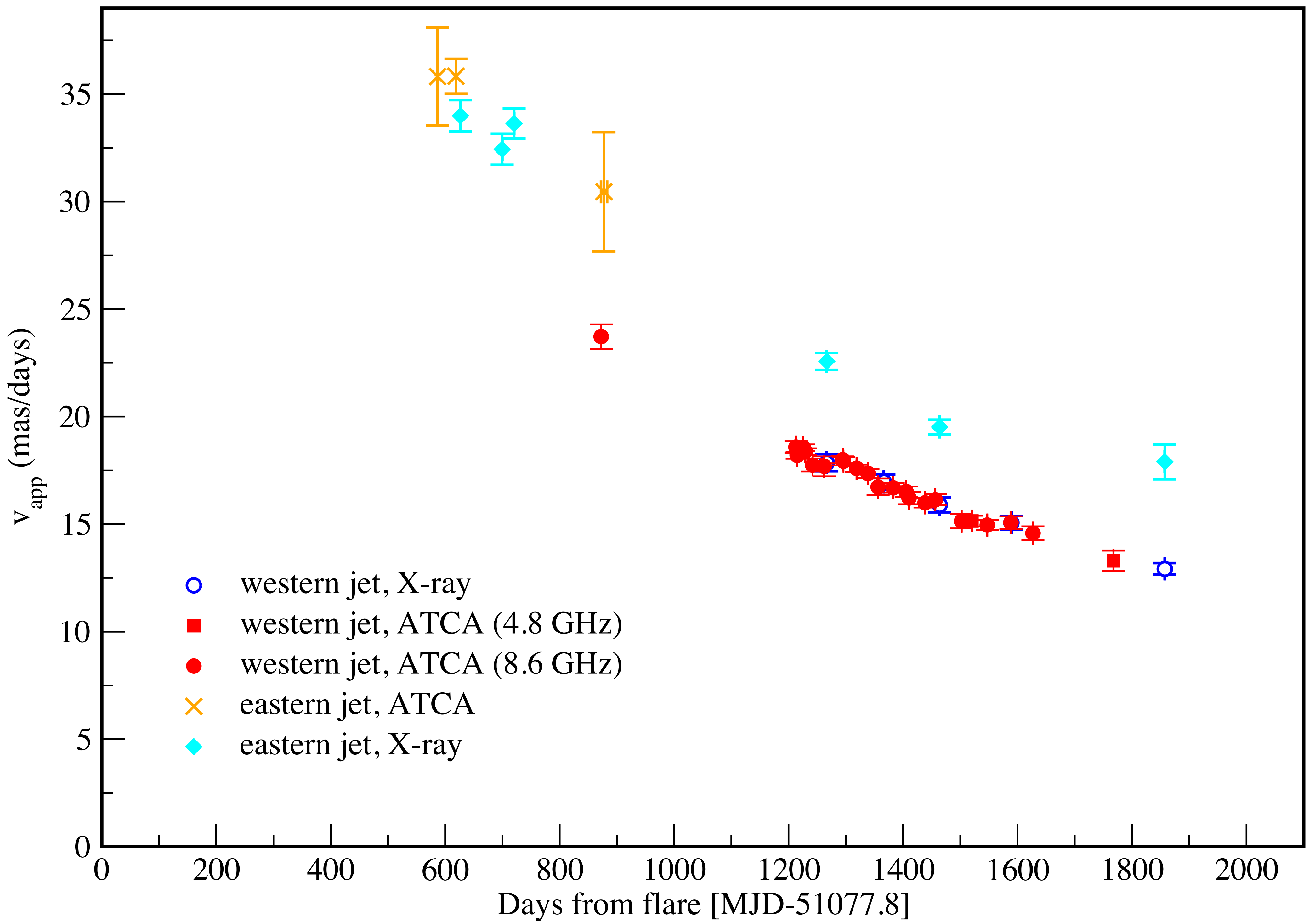

XTE J1550-564 Jets: Dynamical Model

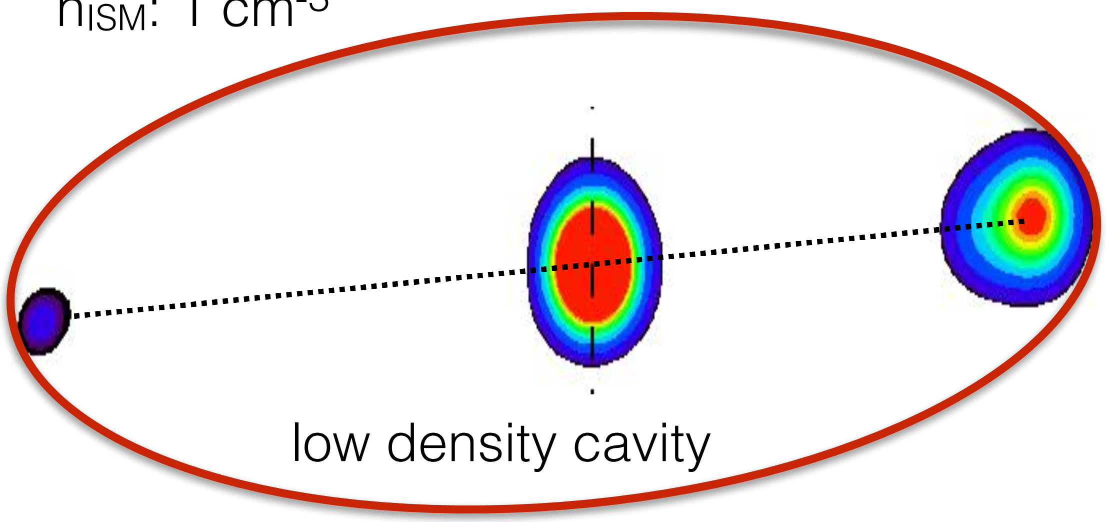

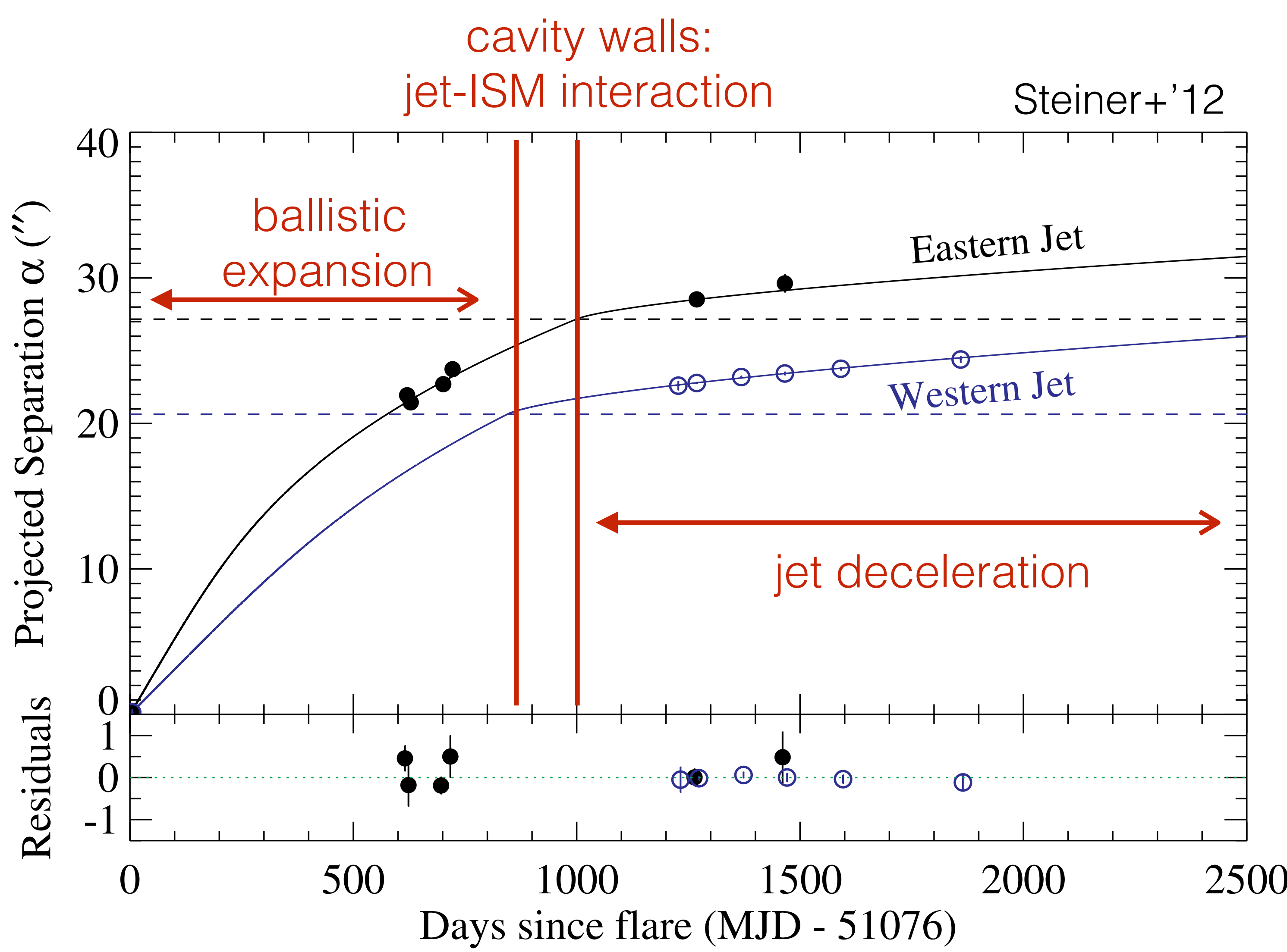

Estimated total energy of the jets is 10^{46} erg (significant fraction of the accreted energy during the 1998 outburst)

Parameter	Model RAC
θ (°)	$72.8^{+7.4}_{-5.4}$
Γ_0	37^{+390}_{-33}
$\tilde{E}^a$ (10^{45} erg)	$6.1^{+3.8}_{-2.3}$
D (kpc)	$4.49^{+0.43}_{-0.35}$
R_{cr} (pc)	0.63 ± 0.06

X-ray Tail: colliding shells

A second outburst in 2000 (Corbel+'01):

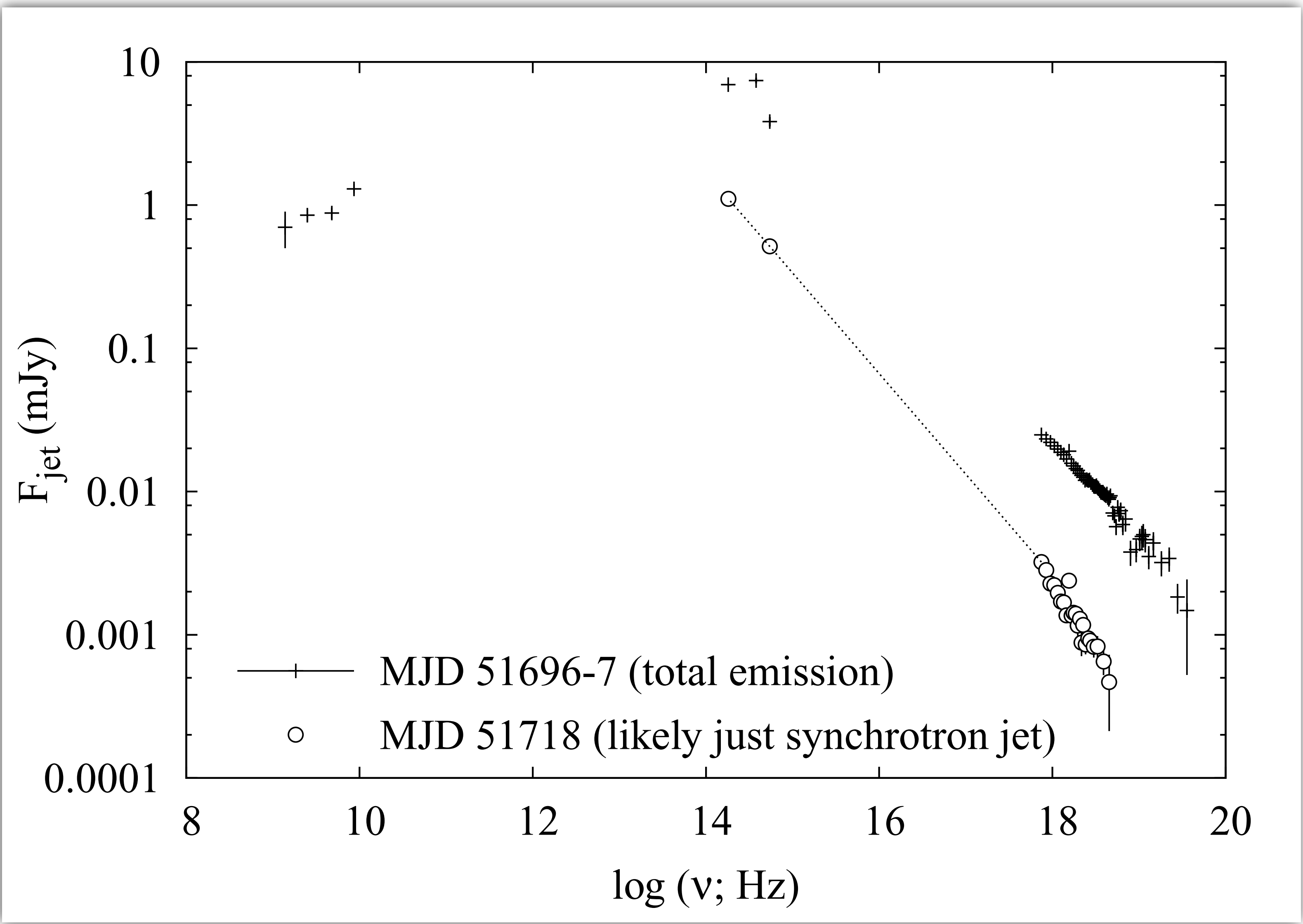

OIR observations support a dominant contribution of the compact jet to the broadband SED (Russell+'10)

Assuming similar travel times (~2 yrs), the new ejecta reached the large scale jet location in ~2002

Eastern & Western Jets: Dynamics

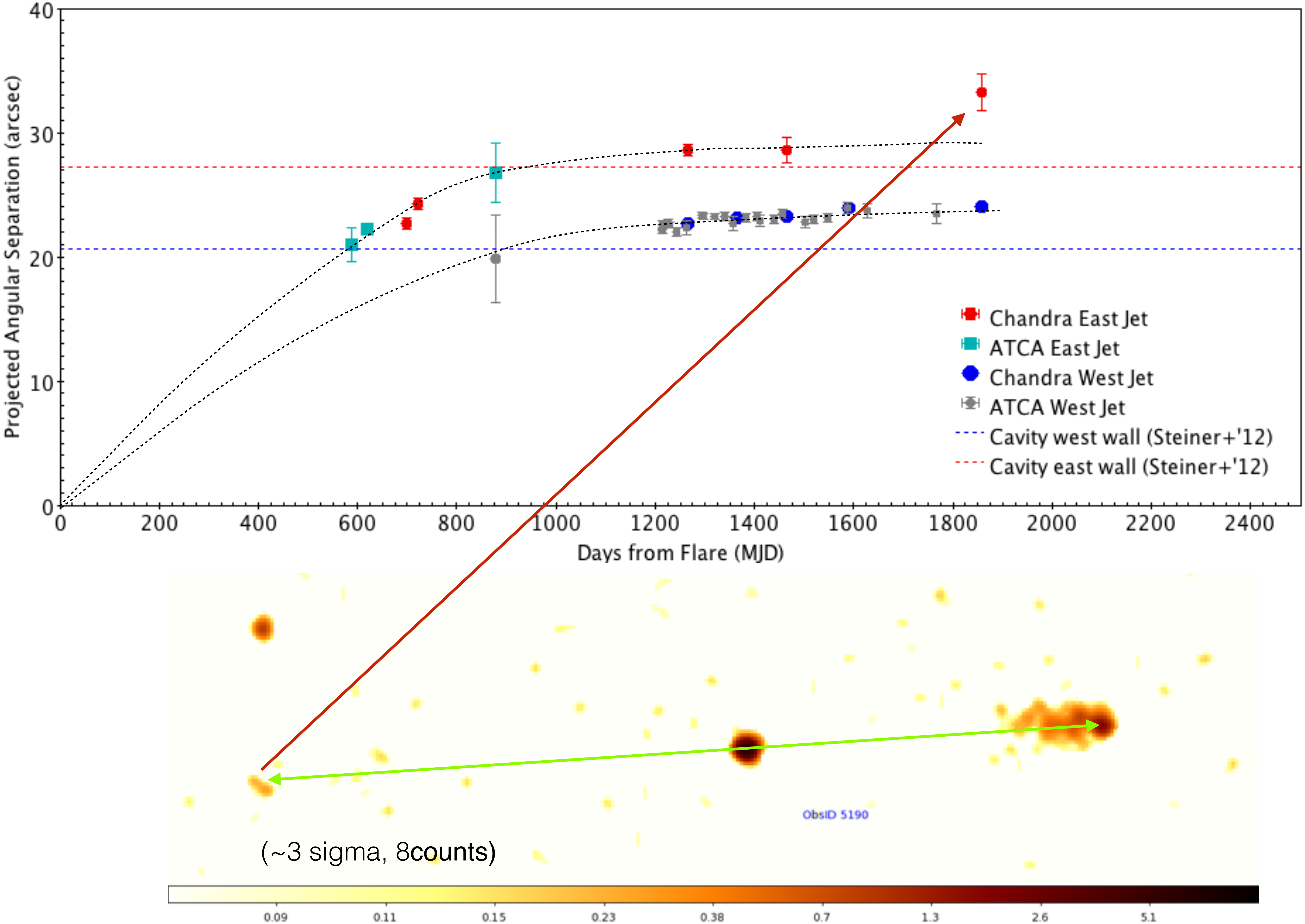

Western Jet: X-ray & radio morphology

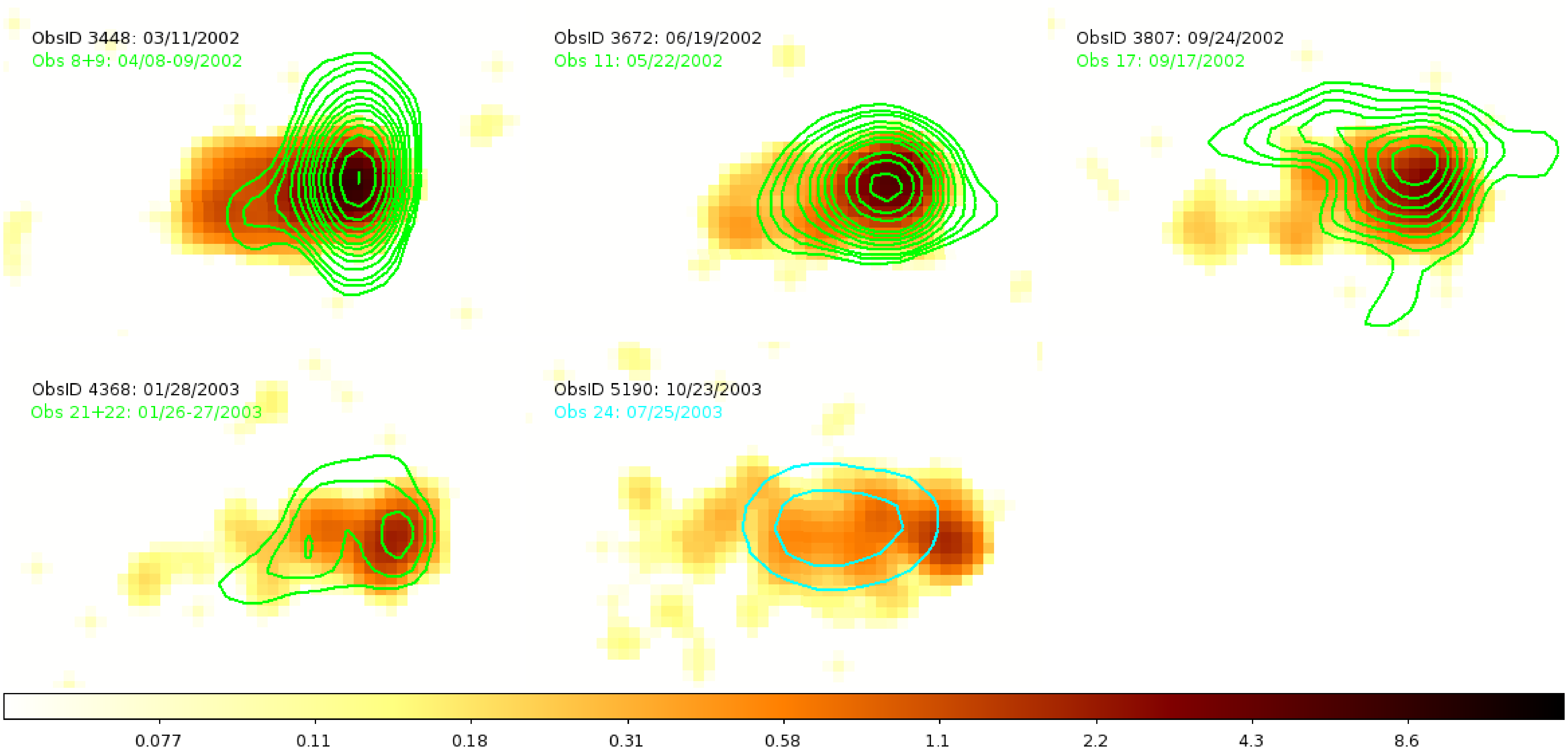

Jet Flavors in Microquasars

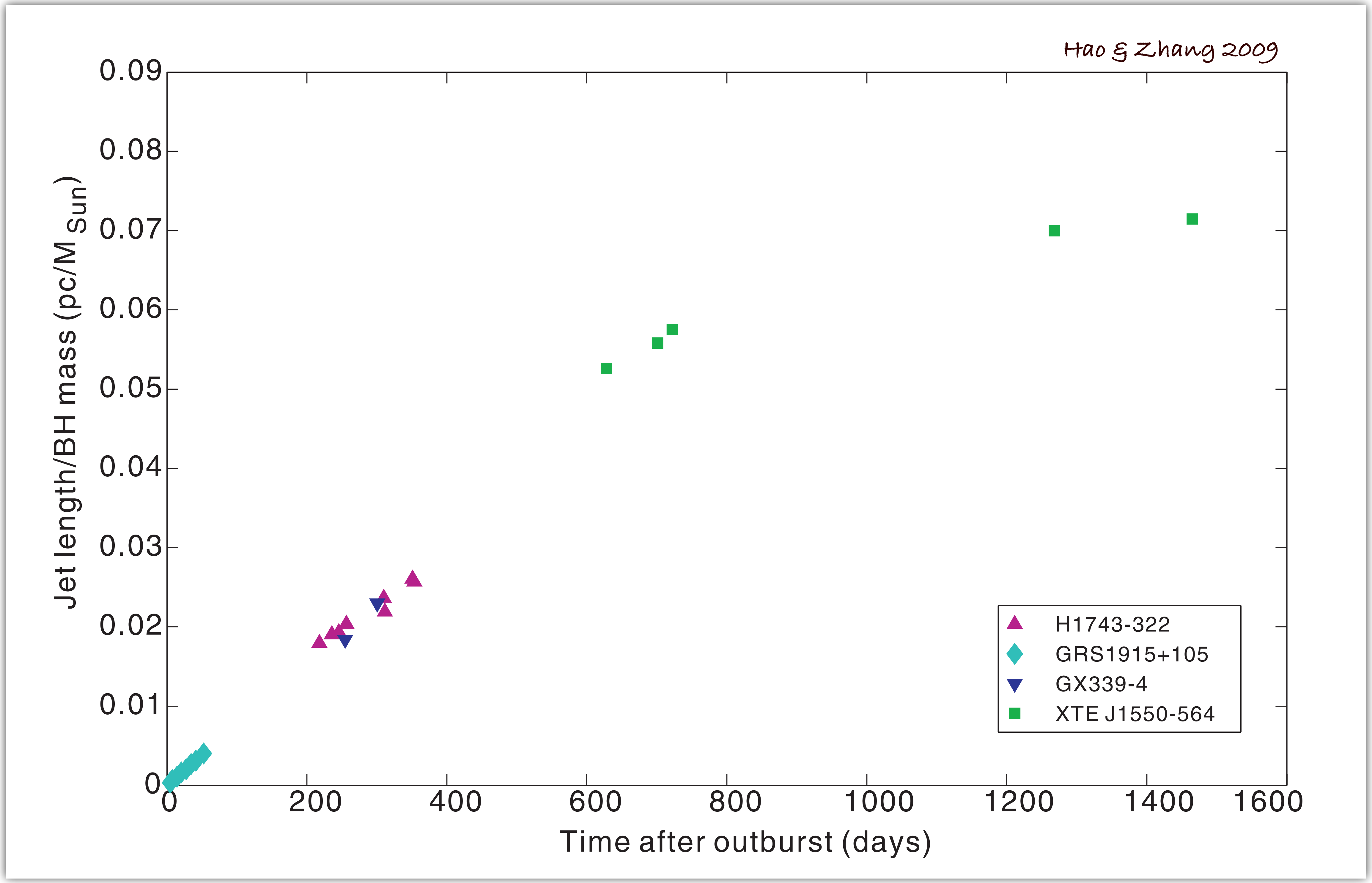

Western Jet: X-ray Morphology

hints of a sinusoidal trajectory?

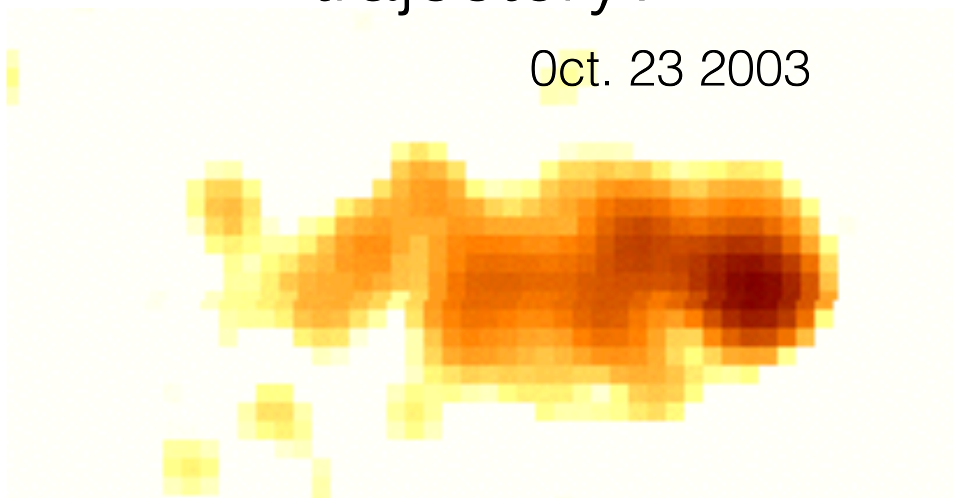

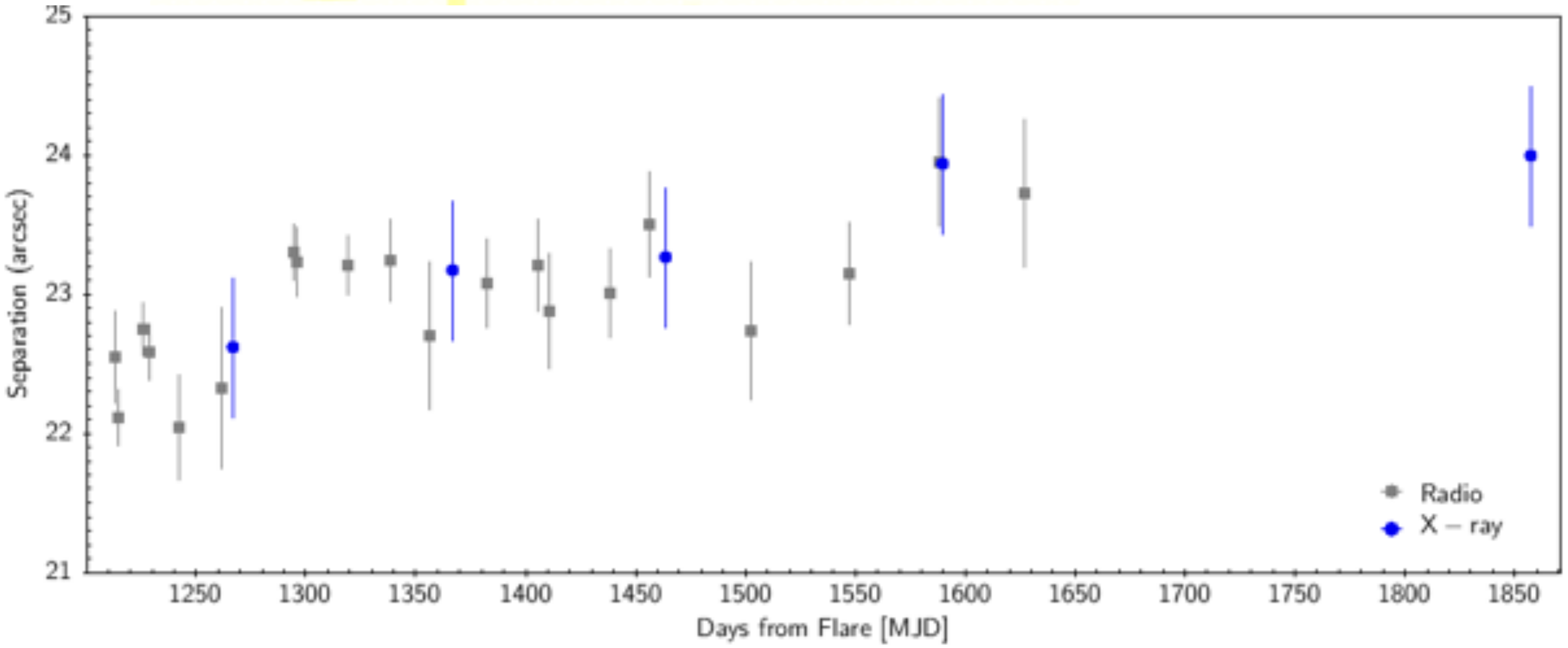

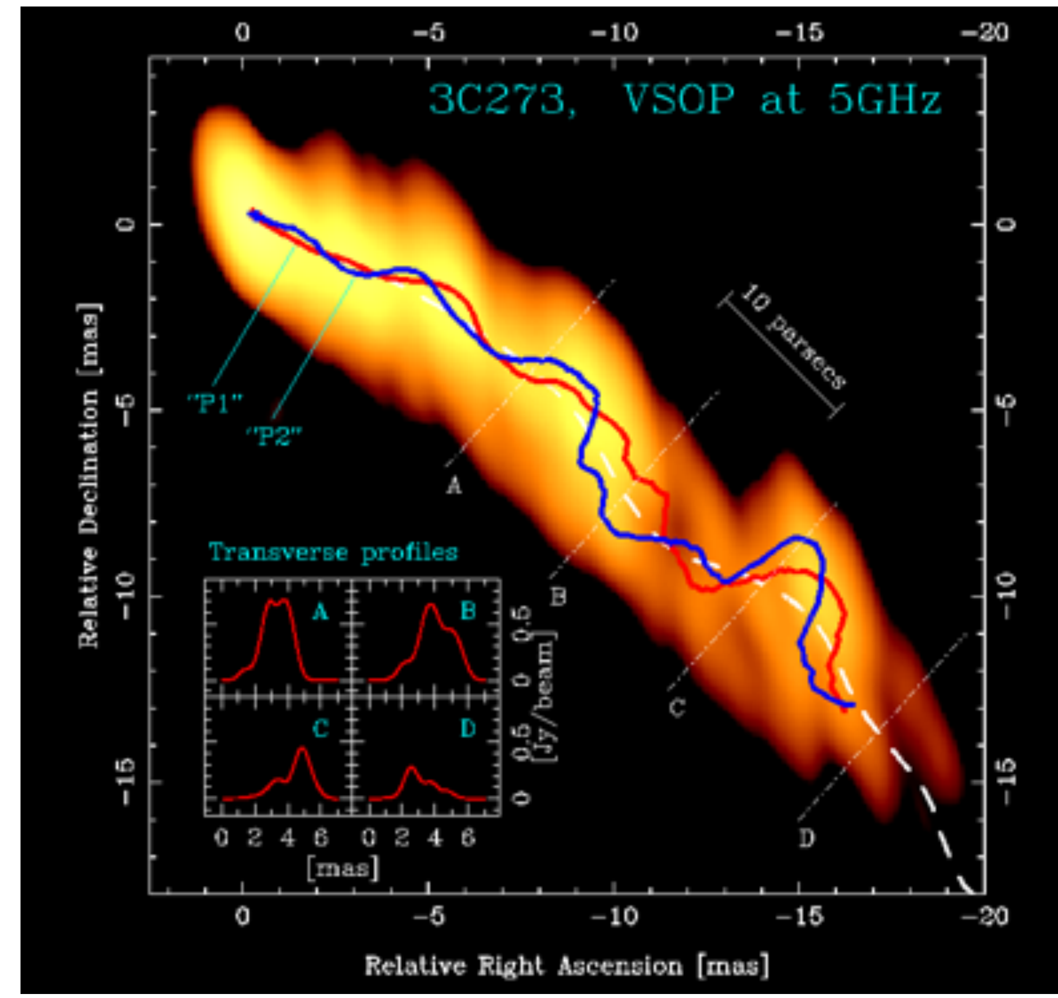

Helical pattern in 3C273 radio jet:
KH instabilities from the jet-ISM interaction
+
initial perturbation

Western Jet in X-rays

ObsID (1)	MJD (days) (2)	Δt (days) (3)	centroid ($''$) (4)	Peak shift[a] ($''$) (5)	Tail pos.[a] ($''$) (6)	$v_{app.,xte}$ (mas days^{-1}) (7)	$v_{app,3448}$ (mas days^{-1}) (8)
3448	52344.62±0.14	1266.81	22.6±0.5	22.75±0.5[b]	19.0	17.9±0.4	–
3672	52444.38±0.10	1366.57	23.2±0.5	0.52±0.12	18.75	17.0±0.4	5.2±1.2
3807	52541.83±0.14	1464.02	23.3±0.5	0.7±0.12	18.25 18*	15.9±0.3	3.5±0.6
4368	52667.19±0.12	1589.38	23.9±0.5	0.85±0.22[c]	18.25 17.75*	15.1±0.3	2.6±0.7
5190	52935.30±0.27	1857.49	24.0±0.5	0.84±0.07[c,d]	16.75 16.5*	12.9±0.3	3.0±1.0[e]

ObsID (1)	Exp. time (2)	Counts (3)	Γ (4)	$norm_{\Gamma,Tot}$ (5)	$F^a_{0.3-8keV,Tot}$ (6)	Γ_{Tail} (7)	$F^a_{0.3-8keV,tail}$ (8)
3448	24.39	414	$1.85^{+0.11}_{-0.10}$	$6.10^{+0.64}_{-0.61}$	$3.46^{+0.17}_{-0.22}$	$2.04^{+0.18}_{-0.40}$	0.8
3672	17.66	238	$1.79^{+0.13}_{-0.14}$	$4.94^{+0.64}_{-0.60}$	$2.90^{+0.19}_{-0.24}$	$1.61^{+0.30}_{-0.30}$	0.5
3807	24.44	197	$2.15^{+0.16}_{-0.14}$	$4.14^{+0.57}_{-0.52}$	$2.05^{+0.17}_{-0.16}$	$2.10^{+0.35}_{-0.35}$	0.4
4368	22.40	110	$1.98^{+0.22}_{-0.21}$	$2.06^{+0.44}_{-0.36}$	$1.12^{+0.11}_{-0.13}$	$2.09^{+0.40}_{-0.40}$	0.4
5190	46.55	145	$1.93^{+0.18}_{-0.18}$	$1.28^{+0.23}_{-0.21}$	$0.62^{+0.04}_{-0.06}$	$1.67^{+0.25}_{-0.25}$	0.36

in units of 10^{-13} ergs cm^{-2} s^{-1}.

Western Jet – ATCA observations: angular separation & apparent velocity.

Obs	MJD days	Separ. arcsec	$v_{app.,xte}$ mas day^{-1}	$v_{app,obs1/01}$ mas day^{-1}
(1)	(2)	(3)	(4)	(5)
		Year 2001		
1/01	51949.99±0.15	20.7±0.5	23.7±0.6	–
		Year 2002		
1	52290.86±0.07	22.55±0.33	18.6±0.3	5.4±1.8
2	52292.86±0.15	22.12±0.20	18.2±0.2	4.1±1.6
3	52303.72±0.12	22.75±0.19	18.6±0.2	5.8±1.5
4	52306.90±0.10	22.58±0.19	18.4±0.2	5.3±1.5
5	52319.73±0.08	22.04±0.38	17.7±0.3	3.6±1.7
6	52339.80±0.08	22.32±0.58	17.7±0.5	4.2±2.0
8	52372.56±0.08	23.30±0.20	18.0±0.2	6.1±1.3
9	52373.71±0.07	23.23±0.25	17.9±0.2	6.0±1.3
10	52396.58±0.17	23.21±0.21	17.6±0.2	5.6±1.2
11	52416.55±0.17	23.24±0.29	17.4±0.2	5.5±1.2
12	52434.30±0.05	22.70±0.53	16.7±0.4	4.1±1.5
13	52460.48±0.12	23.08±0.31	16.7±0.2	4.6±1.1
14	52483.38±0.11	23.21±0.33	16.5±0.2	4.7±1.1
15	52488.41±0.09	22.87±0.41	16.2±0.3	4.0±1.2
16	52516.29±0.17	23.00±0.32	16.0±0.2	4.1±1.0
17	52534.20±0.10	23.50±0.37	16.1±0.3	4.8±1.1
18	52580.17±0.11	22.74±0.50	15.1±0.3	3.2±1.1
19*	52598.12±0.12	23.02±0.38	15.1±0.2	3.7±1.0
20	52624.96±0.11	23.14±0.36	15.0±0.2	3.6±0.9
		Year 2003		
21+22	52666.33±0.33	23.94±0.46	15.1±0.3	4.5±0.9
23	52704.81±0.06	23.72±0.53	14.6±0.3	4.0±1.0
24*	52845.49±0.07	23.50±0.84	13.3±0.5	3.1±1.1

GRB afterglow models:
forward & reverse shock emission

early afterglow:

reverse shock dominated

forward shock dominated